QFlux: An Open-Source Toolkit for Quantum Dynamics Simulations on Quantum Computers. Part IV - Dilation Method for Open Quantum Systems

Xiaohan Dan[1], Saurabh Shivpuje[2], Yuchen Wang[2], Delmar G A Cabral[1], Brandon C Allen[1], Pouya Khazaei[3], Alexander V Soudackov[1], Zixuan Hu[2], Ningyi Lyu[1], Eitan Geva[3], Sabre Kais[4], Victor S Batista[1,5]

1. Department of Chemistry Yale University
2. Department of Chemistry Purdue University
3. Department of Chemistry University of Michigan
4. Department of Electrical and Computer Engineering North Carolina State University
5. Yale Quantum Institute Yale University

Abstract

Energy and charge transfer processes, which are central to photosynthesis, catalysis, and molecular electronics, are governed by quantum dynamics in contact with complex environments. Interactions with surrounding degrees of freedom give rise to dissipation, decoherence, and energy exchange, shaping the mechanisms that determine chemical reactivity and transport phenomena. In Part IV of the QFlux tutorial series, we extend our study of quantum dynamics to open quantum systems, where time evolution is intrinsically non-unitary. Using the Lindblad master equation as a unifying and practical framework, we show how environmental effects can be modeled, simulated, and visualized with QFlux, an open-source platform that bridges classical and quantum computation. The tutorial presents the theoretical foundations of open-system dynamics, constructs the Lindblad propagator, and implements representative simulations ranging from spin models to chemically relevant double-well potentials. Special attention is given to dilation methods, which embed non-unitary dynamics within an enlarged unitary space through ancillary qubits, enabling open-system simulations on quantum hardware. This installment provides both conceptual insight

and computational methodology for exploring dissipative quantum dynamics, laying the groundwork for subsequent parts addressing variational, non-Markovian approaches.

QFlux: An Open-Source Toolkit for Quantum Dynamics Simulations on Quantum Computers. Part IV – Dilation Method for Open Quantum Systems

Xiaohan Dan,[†] Saurabh Shivpuje,[‡] Yuchen Wang,[‡] Delmar G. A. Cabral,[†] Brandon C. Allen,[†] Pouya Khazaei,[¶] Alexander V. Soudackov,[†] Zixuan Hu,[‡] Ningyi Lyu,[†] Eitan Geva,[¶] Sabre Kais,[∗,§] and Victor S. Batista[∗,†,∥]

†Department of Chemistry, Yale University, New Haven, CT 06520, USA

‡Department of Chemistry, Purdue University, West Lafayette, Indiana 47907, USA

¶Department of Chemistry, University of Michigan, Ann Arbor, MI 48109, USA

§Department of Electrical and Computer Engineering, Department of Chemistry, North Carolina State University, Raleigh, North Carolina 27606, USA

∥Yale Quantum Institute, Yale University, New Haven, CT 06511, USA

E-mail: skais@ncsu.edu; victor.batista@yale.edu

Abstract

Energy and charge transfer processes, which are central to photosynthesis, catalysis, and molecular electronics, are governed by quantum dynamics in contact with complex environments. Interactions with surrounding degrees of freedom give rise to dissipation, decoherence, and energy exchange, shaping the mechanisms that determine chemical reactivity and transport phenomena. In Part IV of the **QFlux** tutorial series,

1

we extend our study of quantum dynamics to *open quantum systems*, where time evolution is intrinsically non-unitary. Using the Lindblad master equation as a unifying and practical framework, we show how environmental effects can be modeled, simulated, and visualized with **QFlux**, an open-source platform that bridges classical and quantum computation. The tutorial presents the theoretical foundations of open-system dynamics, constructs the Lindblad propagator, and implements representative simulations ranging from spin models to chemically relevant double-well potentials. Special attention is given to *dilation methods*, which embed non-unitary dynamics within an enlarged unitary space through ancillary qubits, enabling open-system simulations on quantum hardware. This installment provides both conceptual insight and computational methodology for exploring dissipative quantum dynamics, laying the groundwork for subsequent parts addressing variational, non-Markovian approaches.

1 Introduction

In chemistry and physics, the environment often plays a role as crucial as the system itself. Electron and proton transfer reactions in solution, charge transport in proteins and at electrode interfaces, energy migration in photosynthetic complexes, superconducting qubits coupled to resonators, and molecular junctions connected to electron leads are all examples in which environmental effects fundamentally shape the observed dynamics.[1–11] Such situations are naturally described as *open quantum systems*, in which the system of interest interacts with a surrounding environment and therefore cannot be treated as isolated.

In earlier parts of this **QFlux**[12] tutorial series, we developed a progressively richer description of quantum dynamics. **Part I** established the foundations of time-dependent propagation using classical methods and emphasized physical intuition and cross-validation. **Part II** translated these ideas to closed-system quantum simulation on qubit-based hardware, while **Part III** introduced the circuit-synthesis tools required to make these simulations executable, including state preparation and unitary decomposition. The present installment,

Part IV, moves beyond closed systems to open systems, where Markovian descriptions of environmental effects play a decisive role in the system dynamics.

For open quantum systems, the system state can no longer be described by a single wavefunction but instead by a *density matrix*,

$$\rho = \sum_n p_n \left| \psi_n \right\rangle\!\left\langle \psi_n \right|, \tag{1.1}$$

which represents a statistical mixture of quantum states $\left| \psi_n \right\rangle$ with probabilities p_n arising from tracing over environmental degrees of freedom. The reduced dynamics of the system are formally written as

$$\rho(t) = \mathcal{G}(t)\,\rho(0), \tag{1.2}$$

where $\mathcal{G}(t)$ is a dynamical propagator acting on density matrices. Unlike the unitary propagators of closed systems, $\mathcal{G}(t)$ is generally non-unitary, reflecting irreversible processes such as relaxation and dephasing that arise from coupling to the environment.

A wide range of theoretical and numerical approaches have been developed to model $\mathcal{G}(t)$, ranging from exact path-integral formulations to master-equation-based techniques.[3,9,13–21] Among these, the Lindblad master equation, originally formulated by Gorini, Kossakowski, Sudarshan, and Lindblad, has become one of the most widely used frameworks.[22,23] This is particularly true in quantum information science, where it offers a balance between physical interpretability and computational efficiency. The Lindblad formalism relies on the *Markovian* assumption that environmental correlations decay rapidly compared to the system dynamics. When this assumption breaks down, for example, in the presence of strong coupling, structured environments, low temperatures, or ultrafast processes, *non-Markovian* effects become important, and memory must be retained explicitly in the dynamical description. The treatment of non-Markovian dynamics will be discussed in **Part VI**.

Simulating open-system dynamics on quantum hardware entails additional challenges. Quantum circuits are inherently unitary: every operation preserves probability and infor-

mation. In contrast, realistic open-system dynamics are fundamentally non-unitary. As a result, non-unitary evolution must be implemented indirectly. Several frameworks have been developed for this purpose, including linear combinations of unitaries (LCU),[20,24,25] dilation-based approaches,[26–30] quantum imaginary time evolution,[31–33] and variational quantum algorithms.[34–37] Each of these techniques reformulates non-unitary dynamics in terms of unitary operations, typically by enlarging the Hilbert space with ancillary qubits or by introducing parametrized circuit ansätze.

In this part of the **QFlux**[12] tutorial, we focus on *dilation methods* for treating non-unitary dynamics. In these approaches, the system is embedded into an extended Hilbert space that explicitly includes ancillary degrees of freedom representing the environment. The combined system and ancillary state evolve unitarily, while the reduced dynamics of the system alone exhibit open-system effects after tracing out the ancilla.

The purpose of this tutorial is to guide readers through the conceptual foundations of simulating open-system dynamics on quantum computers. We begin by reviewing quantum algorithms for treating non-unitary processes within the quantum-circuit framework. These ideas are then illustrated through a sequence of examples of increasing complexity, ranging from simple spin-$\frac{1}{2}$ models to spin chains and chemically relevant double-well systems. Each example is first analyzed using classical simulations to develop physical intuition and establish reference results, and is subsequently implemented using quantum-circuit-based constructions to highlight algorithmic structure and performance considerations.

All simulations presented here are performed using **QFlux**,[12] the open-source framework introduced in **Part I**. QFlux integrates classical solvers, tensor-network techniques, and quantum-circuit backends within a unified workflow, enabling systematic comparison, validation, and visualization of environmental effects. By working through the examples in this part, readers will acquire the tools needed to determine when open-system treatments are required and to implement them efficiently in realistic quantum simulations.

This installment also prepares the ground for the final parts of the tutorial series. **Part V**

introduces adaptive variational algorithms for the efficient approximate simulation of open-system dynamics on noisy intermediate-scale quantum hardware. **Part VI** builds directly on the framework developed here to explore generalized quantum master equations describing non-Markovian memory effects in chemically and physically realistic environments. Together, these parts complete a coherent pathway from foundational open-system concepts to state-of-the-art quantum simulation methods for complex environments.

2 Quantum algorithm for open system dynamics

Quantum computers natively implement unitary operations, whereas the dynamics of open quantum systems are inherently non-unitary due to dissipation and decoherence. This mismatch presents a central challenge for simulating realistic quantum dynamics on quantum hardware. The dilation method resolves this issue by embedding non-unitary evolution into a higher-dimensional unitary process using ancillary qubits, enabling open-system dynamics to be simulated within standard quantum circuit frameworks. From a physical perspective, dilation mirrors the idea that irreversible behavior emerges when a system is viewed as part of a larger, closed system that includes environmental degrees of freedom. In this section, we demonstrate how to perform quantum simulations of non-unitary evolution in open systems using the dilation method.

2.1 Encoding the density matrix into qubit state vector

To simulate the dynamics governed by Eq. (1.2) in a quantum circuit, it is necessary to encode the information of the density matrix into the state vector of a qubit register. Here, we introduce two commonly used approaches: one is based on vectorization of the density matrix, and the other relies on the Kraus operator representation of open system dynamics.

2.1.1 Vectorization of the density matrix

For a system with an N-dimensional Hilbert space, the density matrix ρ is an $N \times N$ matrix. In the vectorized representation of the density matrix, it is reshaped into an N^2-dimensional vector:

$$\rho \to |\nu_\rho\rangle = [\rho_{11}, \ldots, \rho_{1N}, \rho_{21}, \ldots, \rho_{2N}, \ldots, \rho_{N1}, \ldots, \rho_{NN}]^\top, \tag{2.1}$$

Here the superscript "$\top$" represents a transpose operation. The vectorized density matrix $|\nu_\rho\rangle$ contains all the information about the system and can be represented using $\log_2(N^2)$ qubits.

In this representation, the time evolution described by Eq. (1.2) becomes

$$|\nu_\rho(t)\rangle = \mathbf{G}(t)|\nu_\rho(0)\rangle, \tag{2.2}$$

where $\mathbf{G}(t)$ is the $N^2 \times N^2$ propagator matrix, which is the matrix representation of the superoperator $\mathcal{G}(t)$ in Eq. (1.2).

The time evolution can then be simulated using a quantum circuit: the qubits are initialized to the vector $|\nu_\rho(0)\rangle$ (if $\langle\nu_\rho(0)|\nu_\rho(0)\rangle \neq 1$, it differs by a normalization factor). Then, a quantum gate $\mathbf{U}_G(t)$, corresponding to the non-unitary matrix $\mathbf{G}(t)$, is constructed using the dilation method introduced below. After applying $\mathbf{U}_G(t)$, the output of the quantum circuit represents the time-evolved vectorized density matrix $|\nu_\rho(t)\rangle$.

2.1.2 The Kraus Operator Representation

Here, we introduce another method to represent the density matrix ρ using qubits. This approach utilizes the Kraus operator representation to evolve the system dynamics. It avoids the need to vectorize the density matrix (state vector of dimension N^2) and instead evolves a state vector in the system's N-dimensional Hilbert space. For cases where the density matrix has a large dimension, this method significantly reduces the number of qubits required for simulation.

The Kraus operator representation expresses the reduced density matrix at time t as a sum over operators applied to the density matrix:[38]

$$\rho(t) = \sum_i M_i(t)\rho(0)M_i^\dagger(t), \tag{2.3}$$

where $M_i(t)$ are the Kraus operators ($N \times N$ matrices) that describe the evolution of the system. Conceptually, the Kraus operator representation expresses open-system dynamics as an ensemble of pure-state evolutions, each corresponding to a physically allowed quantum operation. These Kraus operators define a mapping from $\rho(0)$ to $\rho(t)$. Since the evolution is a physical quantum operation, this mapping must be a completely positive map.[38] According to Kraus' theorem, this implies that[38]

$$\sum_i M_i^\dagger M_i \leq I\,, \tag{2.4}$$

with I as the identity matrix. When the "$<$" inequality holds here, it means that the matrix $I - \sum_i M_i^\dagger M_i$ is positive definite.

With the initial density matrix as in Eq. (1.1), $\rho(0) = \sum_n p_n(0) |\psi_n(0)\rangle\langle\psi_n(0)|$, Eq. (2.3) becomes

$$\begin{aligned}\rho(t) &= \sum_{in} p_n(0)M_i(t) |\psi_n(0)\rangle\langle\psi_n(0)| M_i^\dagger(t) \\ &= \sum_{in} p_n(0) \left|\psi_n^i(t)\right\rangle\!\left\langle\psi_n^i(t)\right|\,,\end{aligned} \tag{2.5}$$

where

$$\left|\psi_n^i(t)\right\rangle = M_i(t) |\psi_n(0)\rangle \tag{2.6}$$

is the state obtained by applying the Kraus operator $M_i(t)$ to the initial state $|\psi_n(0)\rangle$.

Therefore, using the Kraus operator representation, the qubits need to be initialized to the state $|\psi_n(0)\rangle$, which involves $\log_2(N)$ qubits. Then, quantum gates $\mathbf{U}_{M_i}(t)$, corresponding to the Kraus operators $M_i(t)$, are constructed using the dilation method. The output of the

quantum circuit represents $|\psi_n^i(t)\rangle$. Then the density matrix is reconstructed via Eq. (2.5).

It is worth noting that the Kraus operator approach requires $\log_2(N)$ qubits to represent the density matrix, compared to $\log_2(N^2)$ in the vectorization method, significantly reducing qubit requirements for large N. However, the trade-off is that multiple circuits need to be executed: the total number of circuits is determined by the product of the number of Kraus operators and the number of quantum states in the expansion of the initial density matrix (i.e., the total number of states $|\psi_n^i(t)\rangle$ for different i and n).

2.1.3 Obtaining the Kraus operators from the propagator matrix

At the theoretical level, the propagator and Kraus representations are equivalent formulations of completely positive open-system dynamics. While the Kraus operator representation in Eq. (2.3) expresses the evolution in terms of an operator-sum decomposition, the propagator matrix $\mathbf{G}(t)$ in Eq. (2.2) provides an explicit linear mapping of the density matrix from time 0 to t.

This equivalence allows the propagator matrix to be systematically converted into a Kraus operator representation. The procedure for performing this transformation, which relies on the Choi–Jamiołkowski isomorphism, is well established in the literature.[18,39,40] Here, we outline the general steps required to obtain the Kraus operators from a given propagator.

First, the Choi matrix[39,40] C is constructed from the propagator $\mathbf{G}(t)$:

$$C = \sum_{i,j=1}^{N} (E_{ij} \otimes I)\mathbf{G}(t)(I \otimes E_{ij}) \tag{2.7}$$

where E_{ij} is an $N \times N$ matrix with the ij-th element equal to 1 and all other elements equal to 0, and I is the $N \times N$ identity matrix. The Choi matrix is a positive definite matrix, which can be diagonalized

$$C = \sum_{k=1}^{N^2} \lambda_k u_k u_k^\dagger \tag{2.8}$$

where $\lambda_k \geq 0$ are the eigenvalues and u_k (dimension $N^2 \times 1$) are the eigenvectors.

After diagonalizing the Choi matrix, the Kraus operators $\{M_k\}$ are constructed by re-shaping $\sqrt{\lambda_k}\, u_k$ into $N \times N$ matrices and taking their conjugate transpose. As indicated in Eq. (2.8), a system with Hilbert-space dimension N admits at most N^2 Kraus operators.

In practice, Kraus operators associated with very small eigenvalues λ_k contribute negligibly to the dynamics. To reduce computational overhead, a tolerance tol_k can be introduced, and all Kraus operators satisfying $\lambda_k < tol_k$ are discarded.

In **QFlux**, this procedure is implemented by diagonalizing the Choi matrix associated with the propagator and retaining only the Kraus operators that satisfy the chosen tolerance criterion. The code for computing the Kraus operators from the propagator matrix is provided in Script S.1.1.

2.2 Dilation Method

As discussed above, both the propagator $\mathbf{G}(t)$ and the Kraus operators $M_i(t)$ are generally non-unitary, reflecting the irreversible nature of open-system dynamics. To implement such dynamics on quantum hardware, where operations must be unitary, we introduce the dilation method, which embeds a non-unitary process-denoted here by M-into a higher-dimensional unitary evolution. This construction is based on Sz.-Nagy's unitary dilation procedure.[41]

For a non-unitary operator M acting on a Hilbert space $\mathcal{H}$, Sz.-Nagy's theorem guarantees the existence of a unitary operator U_M defined on an enlarged Hilbert space such that the action of U_M, when restricted to $\mathcal{H}$, reproduces the action of M. In particular, the 1-dilation yields a unitary operator of the form

$$U_M = \begin{pmatrix} M & D_{M^\dagger} \\ D_M & -M^\dagger \end{pmatrix}, \qquad D_M = \sqrt{I - M^\dagger M}, \quad D_{M^\dagger} = \sqrt{I - MM^\dagger}. \qquad (2.9)$$

Here, D_M and $D_{M^\dagger}$ are referred to as defect operators. The 1-dilation doubles the dimension of the Hilbert space, corresponding to the introduction of a single ancillary qubit in a quantum circuit. Since the defect operators involve the square root of $I - M^\dagger M$, the

operator M must be a *contraction*, meaning that its operator norm satisfies

$$\|M\|_{\text{op}} = \sup_{\boldsymbol{v} \neq 0} \frac{\|M\boldsymbol{v}\|}{\|\boldsymbol{v}\|} \leq 1. \tag{2.10}$$

Conceptually, the dilation method embeds irreversible open-system dynamics into a larger, closed system whose total evolution is unitary, while non-unitary behavior emerges in the reduced dynamics after tracing out the ancillary degrees of freedom (DOF's). At the circuit level, this construction is realized by introducing an ancillary qubit and implementing a unitary gate acting on the combined system–ancilla space.

In practice, when M is a Kraus operator, as shown in Eq. (2.4), it is a contraction. When M is the propagator matrix $\mathbf{G}(t)$, one can divide the original $\mathbf{G}(t)$ by a norm n_d, ensuring that the rescaled $\mathbf{G}(t)$ is a contraction (this norm n_d will be multiplied back when obtaining the final result).

We can verify the relation $U_M^\dagger U_M = U_M U_M^\dagger = I$ and for any vector v in $\mathcal{H}$,

$$U_M \begin{pmatrix} \boldsymbol{v} \\ \boldsymbol{0} \end{pmatrix} = \begin{pmatrix} M\boldsymbol{v} \\ \boldsymbol{v}' \end{pmatrix}, \tag{2.11}$$

which implies that after disregarding $\boldsymbol{v}'$ in the extended space, U_M yields the same results as M.

We implement the Sz.-Nagy dilation function in Script S.2.1. This 1-dilation technique has been applied to simulating open quantum system dynamics.[27,42–44] More advanced dilation schemes have recently been developed, leveraging the singular-value decomposition (SVD) of the operator M to express it as a sum of two unitary operators.[29] This approach outperforms the traditional LCU method and reduces circuit depth compared to Sz.-Nagy dilation.[18,21,29] Moreover, combining SVD dilation with the Walsh operator representation of diagonal unitary operators[45] further simplifies circuit implementation.[18] These techniques are detailed in Ref. 21 and have been integrated into the **QFlux** package. As illustrated in

, users can specify different dilation methods to construct quantum circuits.

2.3 Quantum Circuit

We now translate the theoretical constructions introduced above into executable quantum circuits. In particular, we show how the dilated forms of the propagator in Eq. (2.2) and the Kraus operators in Eq. (2.6) can be implemented as unitary gates acting on an extended Hilbert space. After dilation, the time evolution of the system is expressed as

$$
\begin{pmatrix} |\nu_\rho(t)\rangle \\ |\nu'(t)\rangle \end{pmatrix} = \mathbf{U}_G(t) \begin{pmatrix} |\nu_\rho(0)\rangle \\ \mathbf{0} \end{pmatrix},
\tag{2.12}
$$

$$
\begin{pmatrix} |\psi_n^i(t)\rangle \\ |\psi'(t)\rangle \end{pmatrix} = \mathbf{U}_{M_i}(t) \begin{pmatrix} |\psi_n(0)\rangle \\ \mathbf{0} \end{pmatrix}.
\tag{2.13}
$$

Here, $\mathbf{U}_G(t)$ and $\mathbf{U}_{M_i}(t)$ denote the unitary dilation of the propagator $\mathbf{G}(t)$ and the Kraus operator $M_i(t)$, respectively. In both cases, the quantum circuit is initialized with the system register prepared in the desired initial state and the ancillary register initialized to the zero state.

At the circuit level, the corresponding unitary gate is then applied to the combined system–ancilla register. After execution of the circuit, the components $|\nu_\rho(t)\rangle$ and $|\psi_n^i(t)\rangle$ encode the time-evolved system information and are accessed through measurement. The remaining components, $|\nu'(t)\rangle$ and $|\psi'(t)\rangle$, reside entirely in the ancillary subspace and are discarded.

In summary, vectorization and Kraus representations offer complementary strategies for encoding open-system dynamics, differing primarily in their qubit requirements and circuit overhead. The dilation method provides a unifying framework that enables both approaches to be implemented as unitary quantum circuits.

3 The Lindblad Master Equation

As a representative model of open-system dynamics, we consider evolution governed by the Lindblad master equation. This equation describes the most general form of a trace-preserving and completely positive dynamical evolution for a system density matrix $\rho(t)$ under the assumptions of Markovianity and weak system-environment coupling. [13,15,46,47] It is given by

$$\frac{\partial \rho(t)}{\partial t} = -\frac{\mathrm{i}}{\hbar} \left[H, \rho(t) \right] + \frac{1}{2} \sum_n \gamma_n \left(2 L_n \rho(t) L_n^\dagger - \rho(t) L_n^\dagger L_n - L_n^\dagger L_n \rho(t) \right), \qquad (3.1)$$

where H is the system Hamiltonian, L_n are Lindblad (jump) operators describing dissipative processes, and $\gamma_n \geq 0$ are the corresponding decay rates. Here, H denotes the Hamiltonian of the isolated system. Interactions with the environment can, in general, modify the system Hamiltonian through the so-called *Lamb shift*. [13] Because these energy shifts are typically small, we neglect this contribution in the following discussion. The operators L_n describe dissipative channels induced by the environment, while the corresponding rates γ_n quantify the strength of these processes.

Although dilation-based constructions can, in principle, encode memory effects through the explicit inclusion of ancillary degrees of freedom, the simulations presented here employ Lindblad-form generators and therefore describe Markovian open-system dynamics. For near-term quantum hardware, simulations must also account for practical limitations such as circuit depth, ancillary qubit requirements, and noise, which can favor approximate or resource-efficient constructions over formally exact realizations.

The derivation of the Lindblad equation is well established and discussed extensively in the literature; [13,15,46] it is not reproduced here. Instead, we specify the relevant forms of H, L_n, and γ_n and focus on simulating the resulting dynamics using both classical and quantum computational approaches.

The Lindblad master equation relies on several standard approximations: [13,15,46,48] *sepa-*

rability, whereby the system and environment are initially uncorrelated and described by a product state; the *Born approximation*, assuming weak system–environment coupling and a large environment that remains effectively unperturbed; the *Markov approximation*, which requires the system evolution timescale to be much longer than the environment correlation time, leading to a memoryless bath; and the *secular approximation*, which neglects rapidly oscillating terms and yields the Lindblad form of the dissipative superoperator.

As shown in Ref. 21, these assumptions limit its applicability. When the Lindblad equation breaks down, numerically exact non-Markovian methods can be employed, which will be discussed in **Part VI** of this tutorial series.

3.1 Solving the Lindblad equation on classical computers

Before delving into the key quantum algorithms in this tutorial, it is crucial to first become acquainted with the numerical simulations that can be performed on classical computers. It is a best practice to run simpler trial examples using numerical simulations before testing quantum algorithms on quantum computers. The results obtained from such simulations, often referred to as "exact results", serve as a benchmark for evaluating the accuracy of quantum algorithms and quantum computers.

In this section, we demonstrate the simulation of the Lindblad master equation, Eq. (3.1), using two methods: matrix exponential propagation and QuTiP's Lindblad master equation solver.[48,49] Using matrix exponential propagation, we can express the Lindblad equation in the form given in Eq. (2.2) and construct the propagator matrix corresponding to the Lindblad equation. The propagator matrix can then be used in the quantum algorithm introduced in Section 2.

3.1.1 Matrix exponential: the propagator of the Lindblad equation

For the first numerical simulation method to solve the Lindblad equation, we present a matrix-vector multiplication approach. This method utilizes commonly used Python pack-

ages `scipy` and `numpy`. The approach involves three key steps: (i) vectorizing the density matrix, (ii) converting the Lindblad equation into a matrix-vector form, and (iii) integrating this matrix-vector equation to determine the system's time evolution.

We can recast the Lindblad equation in Eq. (3.1) in the equivalent matrix-vector form:

$$\frac{\partial \left|\nu_\rho(t)\right\rangle}{\partial t} = -\mathrm{i}H_{\mathrm{eff}} \left|\nu_\rho(t)\right\rangle \quad , \tag{3.2}$$

where $\left|\nu_\rho(t)\right\rangle$ is the vectorized density matrix defined in Eq. (2.1). The effective Hamiltonian is $H_{\mathrm{eff}} = H_C + \mathrm{i}H_D$, with H_C and H_D representing the $N^2 \times N^2$ matrix forms of the commutator and the Lindbladian dissipator in Eq. (3.1), respectively:

$$\begin{aligned} H_C &= H \otimes \mathbb{I} - \mathbb{I} \otimes H^T \quad , \\ H_D &= \frac{1}{2}\sum_n \gamma_n \left[2L_n \otimes L_n^* - \mathbb{I} \otimes L_n^T L_n^* - L_n^\dagger L_n \otimes \mathbb{I} \right] \quad , \end{aligned} \tag{3.3}$$

Here, L_n^* is the complex conjugate of L_n and $\mathbb{I}$ is the identity matrix in the Hilbert space of the Hamiltonian H.

By integrating Eq. (3.2), the density matrix at time t can be expressed as the action of the exponential of the matrix $-\mathrm{i}H_{\mathrm{eff}}$ on the vectorized density matrix at $t = 0$,

$$\left|\nu_\rho(t)\right\rangle = \mathbf{G}(t)\left|\nu_\rho(0)\right\rangle = e^{-\mathrm{i}H_{\mathrm{eff}}t}\left|\nu_\rho(0)\right\rangle \quad . \tag{3.4}$$

Now the Lindblad equation is written in the form of Eq. (2.2) and the propagator matrix $\mathbf{G}(t)$ evolves the system over time. The method for calculating the propagator matrix $\mathbf{G}(t)$ is implemented in Script S.3.1, while the propagation of the Lindblad equation using the matrix exponential is encapsulated in the Python function `propagate_matrix_exp`, as shown in Script S.3.2. A further demonstration of how to call this function and plot the results is provided in Section 4.1.

3.1.2 QuTiP's Lindblad master equation solver

Another convenient way to obtain numerically exact solutions of the Lindblad equation is using QuTiP,[48,49] an open-source software with a predefined Lindblad master equation solver called `mesolve`. This solver uses an ordinary differential equation solver to handle the Lindblad equation, requiring users to provide only the essential parameters and output instructions. The package manages all computational processes, delivering the final results efficiently.

When using `mesolve`, key components must be provided as input: the system Hamiltonian H, the initial density matrix $\rho(0)$, a list of time points for dynamical simulation, and *collapse operators* `c_ops`, defined as $\sqrt{\gamma_n}L_n$. If no collapse operators are given, the solver propagates the Liouville equation of the system (pure system evolution). Additionally, users must specify the output instructions, particularly the operators `e_ops` whose expectation values are to be calculated. With these quantities defined, `mesolve` generates time-dependent expectation values for the given operators by propagating either the Liouville equation or the Lindblad master equation. Execution of both scenarios is shown in Script S.3.3, with the results alongside those obtained from the matrix exponential method in Section 4.1.

4 The Spin-1/2 System

4.1 Simulations on Classical Computers

To illustrate the application of the two numerical methods introduced in Section 3.1, we consider a simple but fundamental example: the spin-$\frac{1}{2}$ system. This system provides a minimal setting for exploring open quantum dynamics and serves as a useful reference point for benchmarking both classical and quantum simulations.

In the absence of environmental coupling, the dynamics of an isolated spin-$\frac{1}{2}$ system are characterized by coherent oscillations, corresponding to sinusoidal population exchange be-

tween the two energy levels. Here, we incorporate environmental effects through dissipative terms in the Lindblad equation, allowing direct comparison between closed- and open-system dynamics. This comparison provides physical intuition for the role of dissipation and establishes reliable classical reference results for subsequent quantum simulations.

The spin-1/2 system can be modeled using the following Hamiltonian:

$$H = E_0 \, \sigma^z + \Delta \, \sigma^x \tag{4.1}$$

where E_0 is the energy splitting between the two spin states, Δ is the tunneling rate, σ^z and σ^x denote the Pauli Z and X matrices, respectively. In this case, we select spin-1/2 system parameters as $E_0 = 0$, $\Delta = 0.1 \times 2\pi$. For the jump operators in Eq. (3.1), we select a single jump operator $L = \sigma^x$ and the damping rate $\gamma = 0.05$.

The spin-up $|\uparrow\rangle$ and spin-down $|\downarrow\rangle$ states, which are the basis states of the system, are defined as:

$$|\uparrow\rangle = |0\rangle = \begin{bmatrix} 1 \\ 0 \end{bmatrix}, \qquad |\downarrow\rangle = |1\rangle = \begin{bmatrix} 0 \\ 1 \end{bmatrix} \tag{4.2}$$

These states represent the two possible spin orientations of a spin-1/2 particle. The initial state of the system is set to the spin-up state:

$$|\psi(0)\rangle = |0\rangle \,, \quad \rho(0) = |0\rangle\langle 0| \;\; . \tag{4.3}$$

These settings for the spin-1/2 system are shown in Script S.4.1.

With the parameters defined above, we can propagate the Lindblad equation to simulate the dynamics and evaluate the expectation value of the Pauli Z matrix, $\langle \sigma^z \rangle(t)$. Similarly, we also solve the closed system Liouville equation for comparison, allowing us to observe the differences between closed and open system dynamics. This is achieved by omitting the specification of the collapse operator when using the `qutip.mesolve` function. These steps are shown in Script S.4.2.

The results are shown in Fig. 1. The dynamics of $\langle \sigma^z \rangle(t)$ described by the Liouville equation with the system Hamiltonian H exhibit persistent oscillations with the frequency $2\sqrt{E_0^2 + \Delta^2}$ known as the Rabi frequency.[14] The jump operator term L in the Lindblad equation introduces dissipation, leading to damped oscillations in the dynamics of $\langle \sigma^z \rangle(t)$. The consistency between the two methods (matrix exponential propagation and QuTiP `mesolve`) indicates the accuracy of our propagation techniques and validates our simulations of the dynamics.

The simulation can also be easily performed using the **QFlux** package, as demonstrated in Script S.4.4, yielding the same results as those shown in Fig. 1.
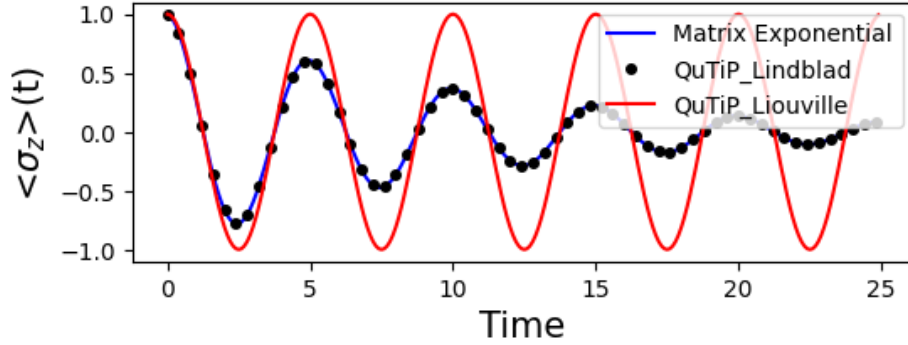
Figure 1: $\langle \sigma^z \rangle(t)$ dynamics of the spin-1/2 system. Here we present results from two methods used to propagate the Lindblad equation (blue curve: matrix exponential propagation; black dots: QuTiP method). The results for the closed system Liouville equation (red curve) are also included for comparison.

4.2 Quantum Simulation: Amplitude Damping Channel

Having established the classical reference dynamics, we now focus on their implementation using quantum circuits constructed within **QFlux**. In this example, we choose parameters for the spin-$\frac{1}{2}$ Hamiltonian in Eq. (4.1) that correspond to the amplitude damping channel commonly studied in quantum information theory.[24,27,29] This channel models physically relevant dissipative processes such as atomic spontaneous emission and T_1 relaxation in nuclear magnetic resonance (NMR) spectroscopy.

Specifically, we set $E_0 = 0$ and $\Delta = 0$. For the Lindblad dynamics, we include a single jump operator, $L = \sigma^+$, corresponding to the Pauli raising operator, with a damping rate $\gamma = 1.52 \times 10^9 \, \text{s}^{-1}$.

The corresponding Lindblad master equation is:

$$\dot{\rho}(t) = \gamma \left[\sigma^+ \rho(t) \sigma^- - \frac{1}{2} \{ \sigma^- \sigma^+, \rho(t) \} \right], \tag{4.4}$$

where $\sigma^\pm = (\sigma^x \pm i\sigma^y)/2$ are Pauli raising and lowering operators, respectively.

The initial density matrix is defined as[24,27,29]

$$\rho(0) = \frac{1}{4} \begin{pmatrix} 1 & 1 \\ 1 & 3 \end{pmatrix}, \tag{4.5}$$

and we calculate the populations in the basis $\{ |0\rangle, |1\rangle \}$ from $t = 0$ to $t = 1000$ ps with a time step of 10 ps.

Script S.4.5 implements the steps for simulating amplitude damping dynamics using the **QFlux** package with the vectorized density matrix representation. We initialize a `DynamicsQ` object and set the measurement qubit states to $|000\rangle$ and $|011\rangle$. According to the vectorization of $\rho(t)$ in the dilated space (Eq. (2.1) and Eq. (2.12)), the amplitudes of these states correspond to the populations of the states $|0\rangle$ and $|1\rangle$ in the spin-1/2 system.

The quantum circuit dilation method can be specified by the user, choosing between the Sz.-Nagy dilation (Section 2.2) or the more advanced SVD dilation, which can be combined with the Walsh operator representation for further optimization.

The results are shown in Fig. 2, where the population dynamics obtained from the quantum simulation align with the dynamics computed using the matrix exponential propagation method on a classical computer (labeled "benchmark" in Fig. 2).

In the following, we provide the code details underlying the **QFlux** package. When performing quantum simulations using **QFlux** based on the vectorized density matrix rep-
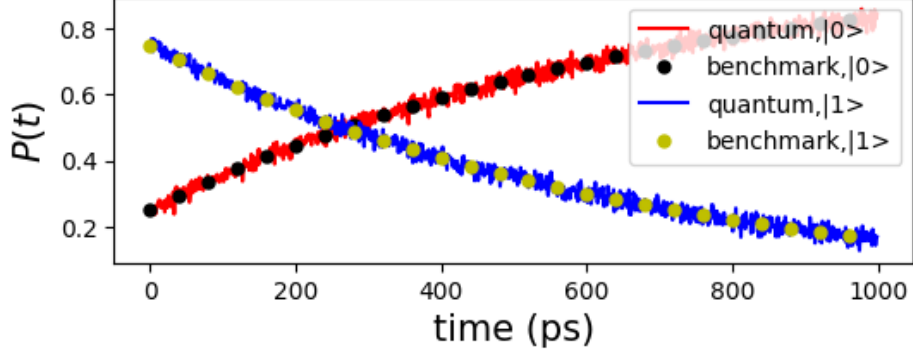
Figure 2: Quantum simulation of the Lindbladian dynamics for the spin-1/2 system with an amplitude damping channel. The population dynamics computed using a quantum simulator (red for $|0\rangle$ and blue for $|1\rangle$) are compared to those obtained from the simulation on a conventional classical computer with matrix exponential propagation (black dot for $|0\rangle$ and yellow dot for $|1\rangle$).

resentation, we first employ the matrix exponential propagation method (Section 3.1) to obtain the propagator for Eq. (4.4), as demonstrated in Script S.4.7. Once the propagator is obtained, it can be directly applied to the initial state vector to generate classical numerical results, which serve as a benchmark for the quantum simulation.

With the propagator $\mathbf{G}(t)$ calculated, **QFlux** performs the dilation and constructs the corresponding quantum circuit for $\mathbf{U}_G(t)$. As an illustrative example, we use the `dilate` function defined in Script S.2.1 to perform the circuit dilation. After executing $\mathbf{U}_G(t)$ and measuring the qubits, the population of the spin-1/2 system in $|0\rangle$ and $|1\rangle$ states can be obtained by taking the square root of the measurement probabilities for the qubit states $|000\rangle$ and $|011\rangle$, followed by applying the normalization factors associated with the dilation and the initial density operator:

$$P_0 = A_0 n_d \sqrt{N_{000}/N} \tag{4.6}$$

$$P_1 = A_0 n_d \sqrt{N_{011}/N} \ , \tag{4.7}$$

where N is the total number of shots, n_d is the norm associated with dilation, and A_0 is the norm of the vectorized initial density matrix. N_{000} and N_{011} are the number of shots at $|000\rangle$

19

and $|011\rangle$, respectively. Script S.4.8 shows the implementation details of the construction and execution of the quantum circuit for the Lindblad dynamics governed by Eq. (4.4). The results are consistent with those obtained from **QFlux** in Script S.4.5.

5   Spin Chain

As another example, we choose the Heisenberg spin-chain model, which is widely used to study the properties of radical and magnetic materials.[50] A schematic representation of a spin-chain model, including its coupling to the environment, is shown in Fig. 3. The Hamiltonian for the spin-chain is defined as follows:[51]

$$H = \sum_{n=0}^{N-1} \Omega_n \sigma_n^z - \frac{1}{2} \sum_{n=0}^{N-2} \left(J_{n,n+1}^x \hat{\sigma}_n^x \hat{\sigma}_{n+1}^x + J_{n,n+1}^y \hat{\sigma}_n^y \hat{\sigma}_{n+1}^y + J_{n,n+1}^z \hat{\sigma}_n^z \hat{\sigma}_{n+1}^z \right) \tag{5.1}$$

where N denotes the number of spins in the model, σ_n^i denotes a Pauli matrix acting on the n-th ($n \in \{0, ..., N-1\}$) spin site with $i \in \{x, y, z\}$. Ω_n is the local potential in the n-th spin site, $J_{n,n+1}^i$ with $i \in \{x, y, z\}$ denotes the coupling between n-th and $(n+1)$-th site.

For illustrative purposes, we consider the parameters as used in the Ref. 51 but with three spin sites ($N = 3$) rather than twenty.

Table 1: Hamiltonian parameters used in the spin chain simulation, from Fiori *et al*[51]

Parameter	$n = 0$	$n \neq 0$
Ω_n	0.65	1.0
$J_{n,n+1}^x$	0.75	1.0
$J_{n,n+1}^y$	0.75	1.0
$J_{n,n+1}^z$	0.0	0.0

The initial state and the corresponding density matrix are defined as

$$|\psi(0)\rangle = |\uparrow\downarrow\downarrow\rangle, \quad \rho(0) = |\psi(0)\rangle\langle\psi(0)| \quad . \tag{5.2}$$

This state is a Kronecker product of the spin-up (first site) and spin-down vectors and the
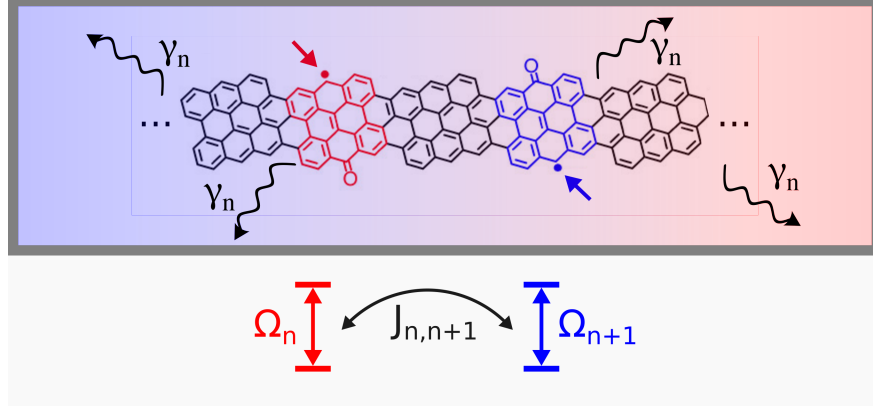
Figure 3: Schematic representation of a spin chain model coupled to an environment, where a graphene nanoribbon acts as a spin chain. The free radical moieties in the polymer group (red or blue molecular groups in the figure) represent the spin sites, which may have spin up or down. Ω_n is the energy required to flip the spin state at the particular polymer site n, and $J_{n,n+1}$ is the offsite couplings between spins at site n and $n+1$. The graphene nanoribbon is coupled to a bath, with the dissipation effect given by the damping rate γ_n (for simplicity $\gamma_n = \gamma_{n+1} \ \forall n$).

initial density matrix is the projector on the initial state vector (since it is a pure state).

We use the Script S.5.1 to set the spin chain's initial state and the Hamiltonian. Likewise, Script S.5.2 defines the spin chain Hamiltonian through the Kronecker product of the Pauli matrices constituting the Hamiltonian operators.

The jump operators for the Lindblad equation of the spin chain were chosen to model the effect of dissipation of an analogous spin system on a quantum device.[52] We rewrite the Eq. (3.1) as

$$\dot{\rho}(t) = -\mathrm{i}[H, \rho(t)] + \frac{1}{2} \sum_{m=1}^{2} \sum_{n=0}^{N-1} \gamma_{m,n} \left[2L_{m,n}\rho(t)L_{m,n}^{\dagger} - \rho(t)L_{m,n}^{\dagger}L_{m,n} - L_{m,n}^{\dagger}L_{m,n}\rho(t) \right] \quad (5.3)$$

Here m denotes two different noise channels, the amplitude damping noise ($m=1$) and the dephasing noise ($m=2$), acting on the n-th spin site. The jump operators $L_{m,n}$ associated

with these noise channels are[52]

$$L_{1,n} = \hat{\sigma}_n^- \tag{5.4}$$

$$L_{2,n} = \hat{\sigma}_n^+ \hat{\sigma}_n^- \quad . \tag{5.5}$$

with $\hat{\sigma}_n^\pm \equiv (\hat{\sigma}_n^x \pm i\hat{\sigma}_n^y)/2$. The damping rates $\gamma_{1,n}$ and $\gamma_{2,n}$ can be experimentally determined by measuring the spin relaxation process.[52] Here, we choose $\gamma_{1,n}$ and $\gamma_{2,n}$ corresponding to the average noise determined by Dang and coworkers in Ref. 52, where they determined the average noise for the two relaxation processes as $T_{1,n} = 24.9 \times 5$ and $T_{2,n} = 15.3 \times 5$ (in units of $1/J$, where J = 5 MHz), with J denoting the nearest-neighbor coupling. Using J has a scale of 1.0 in our Table 1, and relate $T_{1,n}$ and $T_{2,n}$ to damping rate through $\gamma_{1,n} = 2/T_{1,n}$, $\gamma_{2,n} = 4/T_{2,n}$, then we have $\gamma_{1,n} = 0.016$ and $\gamma_{2,n} = 0.0523$. With the jump operators and damping rates defined, we can implement it in a manner analogous to the spin chain Hamiltonian. For convenience, we store the collapse operators $\sqrt{\gamma_{m,n}}L_{m,n}$.

The observable of interest for our spin chain example is the survival amplitude, defined as

$$A_s(t) = \sqrt{\mathrm{Tr}[\rho(t)\rho(0)]} \quad , \tag{5.6}$$

When starting from a pure state $|\psi(0)\rangle$, this expression is equal to $|\langle\psi(0)|\psi(t)\rangle|$.

5.1 Classical Simulation

The Lindblad dynamics for the spin chain can be simulated with the matrix exponential propagation method and the QuTiP method. Similar to the single spin-1/2 case, we propagate the pure system Liouville equation for comparison.

The results are shown in Fig. 4. The dynamics of the pure system Liouville equation demonstrates that the system oscillates between different spin configurations and recovers the initial state after some time. However, the Lindblad equation includes the spin relaxation process which is described by two types of jump operators. This leads to the relaxation of

the survival amplitude and the initial state is not recovered. Similar to the spin-1/2 case, the matrix exponential propagation and QuTiP `mesolve` give the same result.
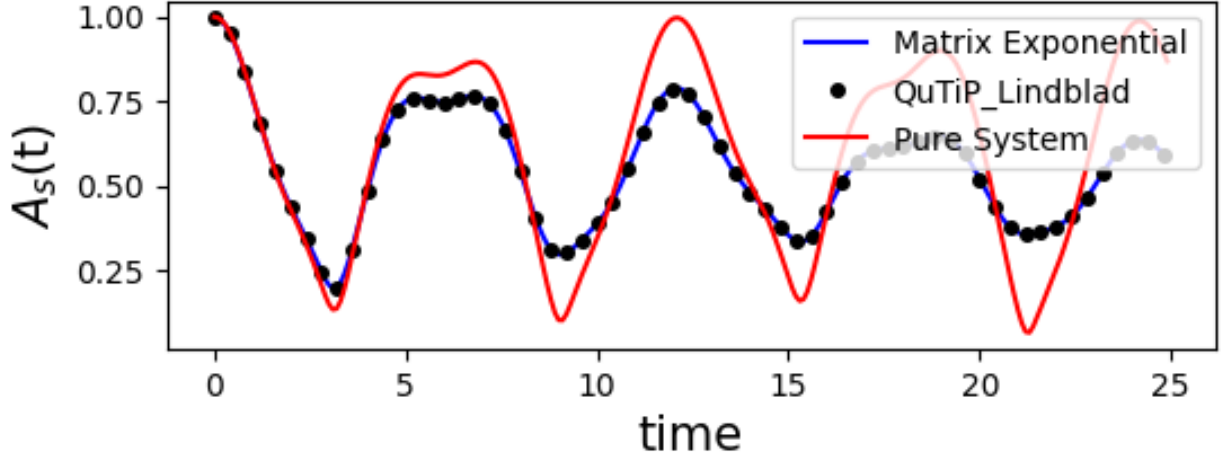

Figure 4: Quantum dynamics of the spin-chain for the pure system evolution (red line) and the open system dynamics described by the Lindblad equation (blue line for matrix exponential propagation and black dot for QuTiP method). Without dissipation, the pure system oscillates between the available spin configurations, while after introducing the spin relaxation process, the system gradually loses energy and deviates from its initial state as the simulation time increases.

By instantiation of a `Dynamics` object corresponding to the spin chain Hamiltonian, the above results can also be simulated using the **QFlux** package. The implementation is provided in Script S.5.6.

5.2   Quantum Simulation

In this subsection, we extend the quantum algorithm to perform the qubit-based simulation of the Lindblad dynamics of the spin chain Hamiltonian. We use the same spin chain parameters as in the conventional computer simulation in Section 5.1.

Similar to the previous example of simulating the spin-1/2 system, the quantum circuit simulation of the spin chain can also be directly performed using the **QFlux** package. Script S.5.7 provides the details of the implementation.

Here, we measure the state $|0011011\rangle$ because, in our specific example, the initial density matrix is given by $\rho(0) = |\uparrow\downarrow\downarrow\rangle\langle\uparrow\downarrow\downarrow| = |011\rangle\langle011|$. Consequently, its vectorized form is $|\nu_\rho(0)\rangle = |011011\rangle$, and the corresponding initial state vector in the dilated space is $|\tilde{\nu}_\rho(0)\rangle = |0011011\rangle$. The survival amplitude in Eq. (5.6) is transformed to

$$A_s(t) = \sqrt{|\langle\tilde{\nu}_\rho(t)|\tilde{\nu}_\rho(0)\rangle|} \tag{5.7}$$

where $\langle\tilde{\nu}_\rho(t)|\tilde{\nu}_\rho(0)\rangle$ can be obtained by taking the square root of the probability of measuring the $|0011011\rangle$ component in the quantum circuit.

It's important to note that to achieve statistically meaningful results, the quantum simulation must be executed multiple times for each time point and then averaged. To demonstrate this, we carried out the simulations using 1000 and 10000 shots, performed using Qiskit's `AerSimulator`.[53] The results are shown in Fig. 5. While both the results agree well with the classical computer benchmark (QuTiP result in Section 5.1), the results obtained from 1000 shots exhibit more noise compared to the data obtained from 10000 shots.
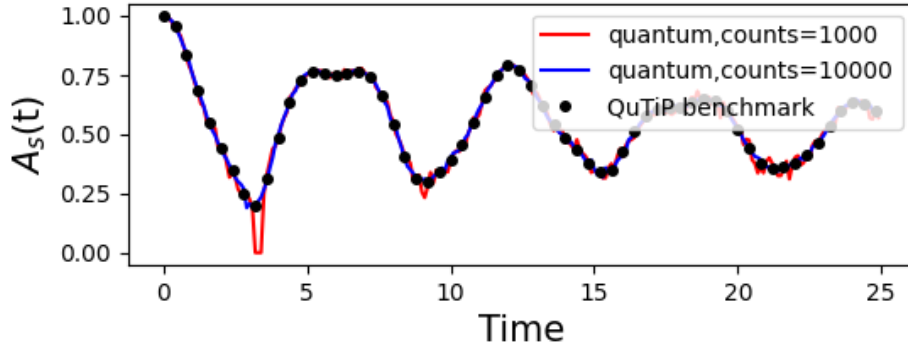

Figure 5: Quantum simulation of the Lindbladian dynamics for the spin-chain model. Two results obtained with different numbers of shots on the quantum device simulator are presented. For comparison, the results from the classical conventional computer simulation using QuTiP (black dots) are also presented.

Script S.5.9 details the implementation of the **QFlux** package. It begins by computing the propagator $\mathbf{G}(t)$ using the method outlined in Section 3.1.1. The quantum circuit is

then initialized at $|\tilde{\nu}_\rho(0)\rangle$, followed by the dilation of the propagator $\mathbf{G}(t)$ to $\mathbf{U}_G(t)$, which is applied to the quantum circuit. Measurements are performed to obtain the dynamics of $A_s(t)$. Note that the normalization factor n_d in the dilation process is applied after the measurement.

6 Double Well

Double-well potentials provide a simple yet powerful model for chemical processes involving barrier crossing, such as proton transfer reactions and conformational changes in molecules. In this context, the two wells correspond to distinct chemical configurations, while population transfer between them reflects reaction dynamics driven by thermal fluctuations and environmental coupling. The time-dependent population of each well can be directly interpreted in terms of reaction rates, with dissipation controlling the timescale over which the system relaxes from a metastable configuration to the energetically favored state.

In this section, we will simulate the Lindblad dynamics in a double-well potential. The double-well form of the potential is ubiquitous in many chemical reactions, such as proton transfer in DNA base pairs[54,55] and proton-coupled electron transfer processes in solution or electrochemical systems.[1,56,57] Since the surrounding environment influences these processes, they are often modeled as a double-well system coupled to a dissipative bath.[58,59] When the system-bath interaction is weak, the Lindblad equation is a suitable choice for such simulations.

Here, we choose the example of proton transfer in DNA base pairs. This dissipative chemical system has been the focus of study in the recent work,[60,61] simulated with an analog quantum processor, yielding reasonable results for chemical kinetics. The system's Hamiltonian H is given by:

$$H = \frac{p^2}{2m} + V(x) \tag{6.1}$$

where p is the proton's momentum, $m = 1836.15$ a.u. is the mass of the proton, and the

model potential $V(x)$ describes the hydrogen bond within the adenine-thymine base pair in DNA:[54,55]

$$V(x) = \alpha \left[0.429 \left(\frac{x}{x_0} \right) - 1.126 \left(\frac{x}{x_0} \right)^2 - 0.143 \left(\frac{x}{x_0} \right)^3 + 0.563 \left(\frac{x}{x_0} \right)^4 \right], \qquad (6.2)$$

Here, x is the one-dimensional proton coordinate defined relative to the middle of the proton transfer interface in an individual adenine-thymine (A-T) pair, $x_0 = 1.9592$ Bohr is the half of the distance between the two minima of the potential, and $\alpha = 0.0367493$ is the unit conversion factor from electronvolts to atomic units. The plot of the potential $V(x)$ is shown in Fig. 6.
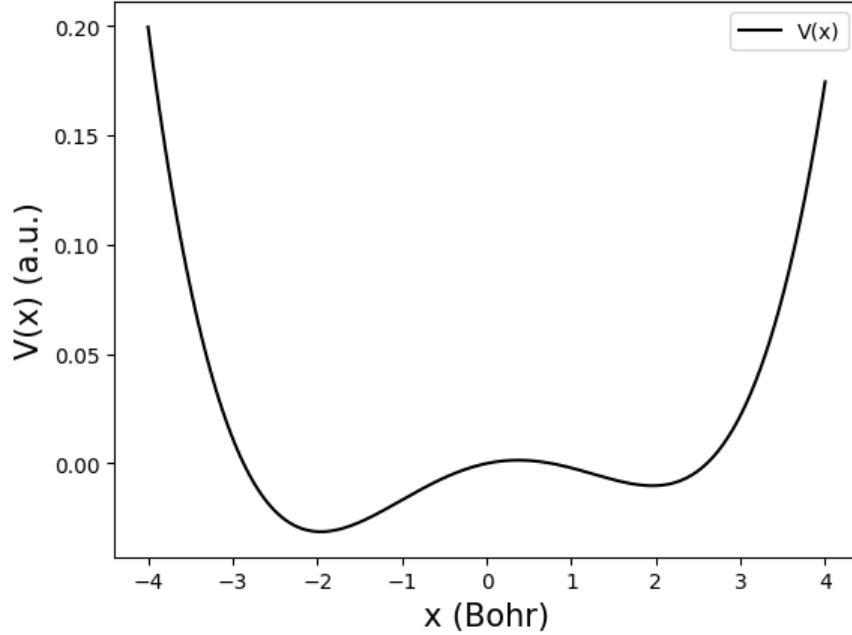
Figure 6: The model double-well potential for the proton motion in the adenine-thymine base pair of DNA.

We can diagonalize the double-well system Hamiltonian H in Eq. (6.1) to obtain the eigenstates:

$$H|\phi_i\rangle = E_i|\phi_i\rangle \qquad (6.3)$$

Here, $|\phi_i\rangle$ represents the i-th eigenstate of the system, and E_i is the corresponding eigenvalue.

The code shown in Script S.6.2 solves for the first $N_{\text{eig}} = 50$ eigenstates of the system. The probability densities for the first 12 eigenstates and the corresponding energy levels are shown in Fig. 7. It can be seen from the figure that the first 10 states are localized in either the left or right well, while the eigenstates after the 11-th are delocalized across the entire double-well potential.

To simulate the proton transfer process, we set the initial state to the eigenstate $|\phi_6\rangle$, which is the first eigenstate localized in the right well:

$$|\psi(0)\rangle = |\phi_6\rangle; \quad \rho(0) = |\psi(0)\rangle\langle\psi(0)| \ . \tag{6.4}$$
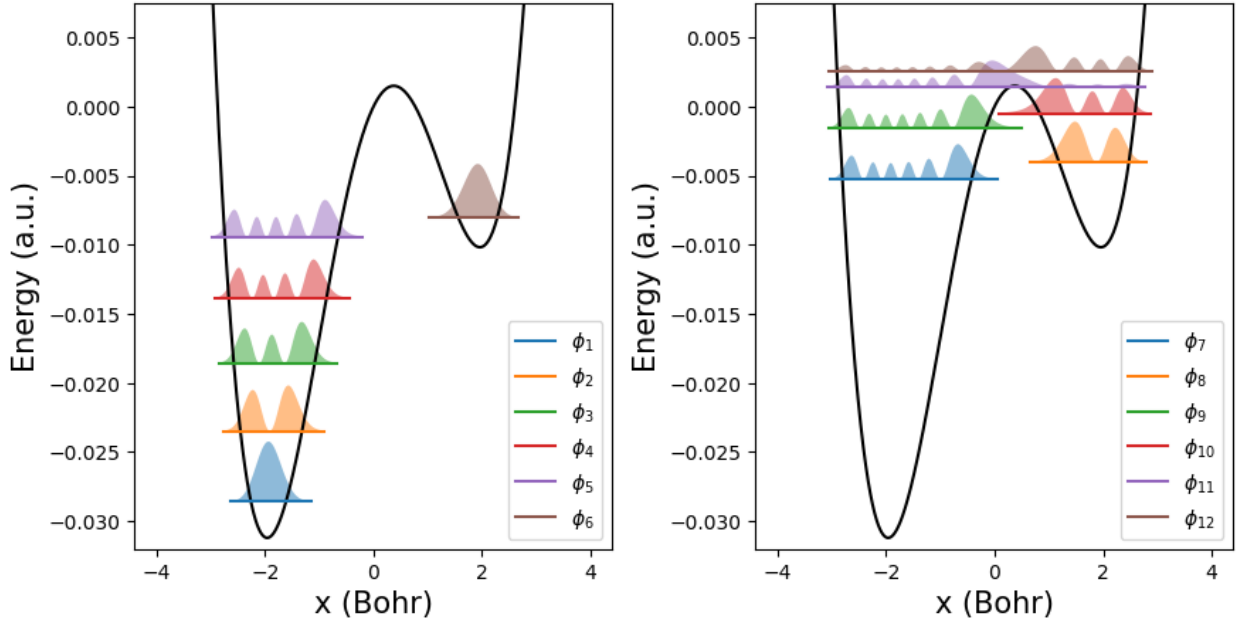
Figure 7: The probability density (scaled by an appropriate scaling factor) for the eigenstates of the system Hamiltonian in Eq. (6.1). The horizontal solid lines indicate the energy levels and the black line shows the double-well potential. The left panel displays the first 6 eigenstates, while the right panel shows the eigenstates from 7 to 12.

The population of the proton in the left (L) and right (R) wells can be characterized by

the following expectation values:

$$P_R = \langle \Theta(x - x^*) \rangle$$

$$P_L = \langle 1 - \Theta(x - x^*) \rangle \ , \tag{6.5}$$

where $\langle A \rangle = \mathrm{Tr}[A\rho]$ for a given operator A, $\Theta(x)$ is the Heaviside function and x^* defines the dividing surface between the left and right wells. Here, $x^* = 0.37321768$ a.u. corresponds to the position at the top of the barrier.

The time evolution of the system is described by the Lindblad equation in Eq. (3.1) with the jump operators L_1 and L_2 that account for the environmental dissipation effects:[62,63]

$$L_1 = \hat{a}$$

$$L_2 = \hat{a}^\dagger \tag{6.6}$$

where $\hat{a}$ and $\hat{a}^\dagger$ are annihilation and creation operators defined as

$$\hat{a} = \sqrt{\frac{m\omega}{2\hbar}}\,\hat{x} + \frac{\mathrm{i}}{\sqrt{2\hbar m\omega}}\,\hat{p} \tag{6.7}$$

$$\hat{a}^\dagger = \sqrt{\frac{m\omega}{2\hbar}}\,\hat{x} - \frac{\mathrm{i}}{\sqrt{2\hbar m\omega}}\,\hat{p} \tag{6.8}$$

Here, the frequency $\omega = 0.00436$ a.u. (956.9 cm^{-1}) corresponds to the bottom of the right well of the double-well potential. We write the specific form of the Lindblad equation for double-well potential as follows:

$$\dot{\rho} = -\mathrm{i}[\hat{H}, \rho(t)]$$

$$+ \kappa\,(1 + n_{\mathrm{th}})\left(\hat{a}\rho(t)\hat{a}^\dagger - \frac{1}{2}\left\{\hat{a}^\dagger\hat{a}, \rho(t)\right\}\right) + \kappa\,n_{\mathrm{th}}\left(\hat{a}^\dagger\rho(t)\hat{a} - \frac{1}{2}\left\{\hat{a}\hat{a}^\dagger, \rho(t)\right\}\right) \tag{6.9}$$

where κ describes the coupling between the system and environment, and $n_{\mathrm{th}} = 1/(\exp(\hbar\omega/k_B T) - 1)$ is the thermally averaged quantum number of the harmonic oscillator corresponding to the temperature of the environment. We choose $\kappa = 1/10$ fs^{-1} and

$T = 300$ K (corresponding to $n_{th} = 0.01$ a.u.).

6.1 Classical Simulation

To propagate the Lindblad equation, we express all operators in the basis of the eigenstates, $\rho_{ij} = \langle \phi_i | \rho | \phi_j \rangle$, $H_{ij} = \langle \phi_i | \hat{H} | \phi_j \rangle$, and similarly for $\hat{a}$ and $\hat{a}^\dagger$. When the basis is truncated to the N_{eig}-th state, these operators are represented as $N_{\text{eig}} \times N_{\text{eig}}$ matrices in the eigenstate basis.

After expressing all operators in the basis of eigenstates, we can use the QuTiP `mesolve` function to simulate the dynamics. Fig. 8 shows the dynamics of the population in the right well. The upper panel presents the results for different eigenstate truncations, and it can be seen that the results converge at $N_{\text{eig}} = 30$. The plot in the top panel shows a comparison between the dynamics simulated using the QuTiP solver and matrix exponential propagation. The good agreement between the two validates our simulation.

It is worth mentioning that using matrix exponential propagation, we can obtain the dynamics at time t directly without iterating over the time steps. In Fig. 9, we present the dynamics of proton transfer on a longer time scale obtained by the matrix exponential. The population $P_R(t)$ exhibits a clear exponential decay. Around 20 ps, the majority of the proton distribution has transferred to the left well. An exponential fit to the data indicates that the rate constant is approximately 8×10^{-2} ps^{-1}. This rate is consistent with dissipative barrier-crossing proton-transfer behavior expected at room temperature.

Fig. 10 provides a spatially resolved view of the population transfer inferred from Fig. 8. By examining the proton probability density at selected time points, the proton transfer process becomes directly visible. As the population $P_R(t)$ in the right well decreases, as shown in Fig. 8, the probability density progressively shifts toward the lower-energy left well.

This spatial redistribution of the proton probability density reflects energy dissipation arising from interactions with the environment. It is important to emphasize that, because

the initial state is an eigenstate of the system Hamiltonian, the population $P_R(t)$ would remain equal to unity and the probability density would remain unchanged in the absence of dissipation. Consequently, the observed proton transfer from the right well to the left well is driven entirely by environmental effects.
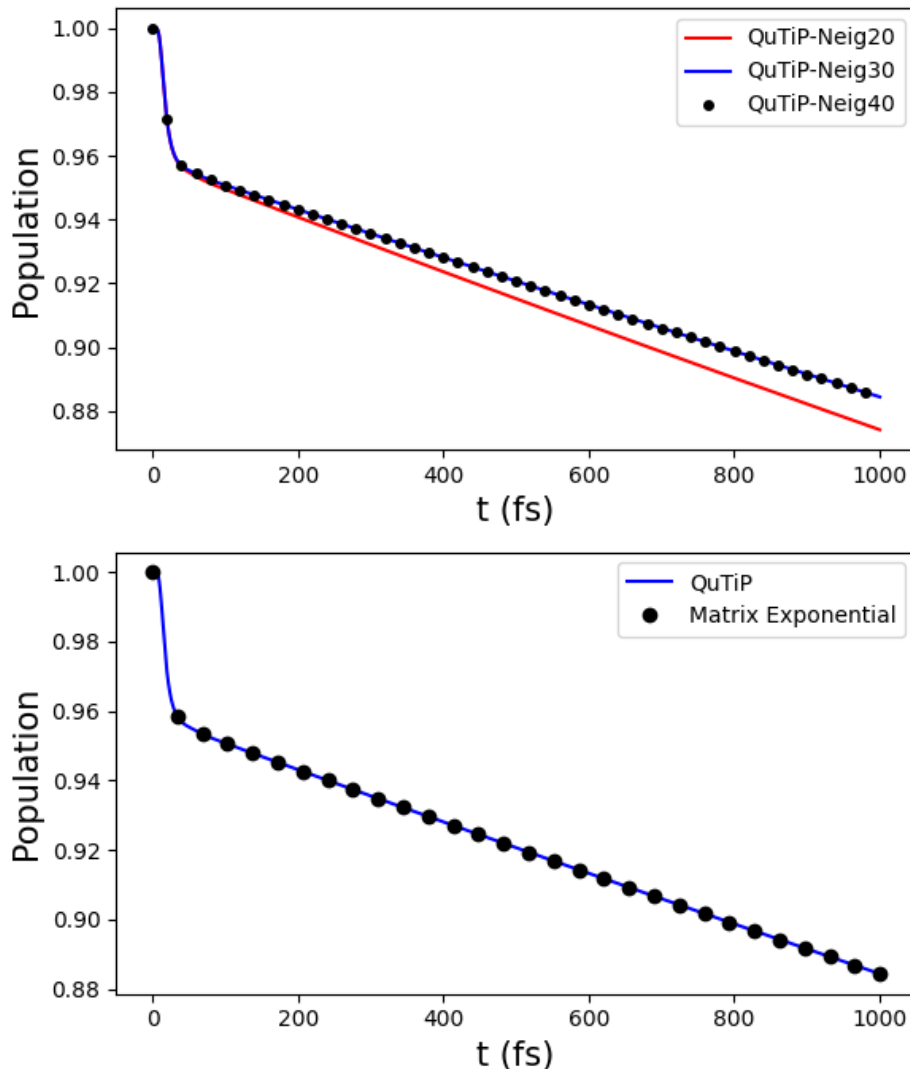

Figure 8: The dynamics of the population in the right well for the double-well system. (Upper) The dynamics simulated with different truncation levels, propagated using QuTiP Lindblad equation solver. (Lower) The results from matrix exponential propagation and QuTiP method, both with the truncation $N_{\text{eig}} = 30$.

The same classical simulation results can also be obtained using the **QFlux** package, with the code provided in Script S.6.5.
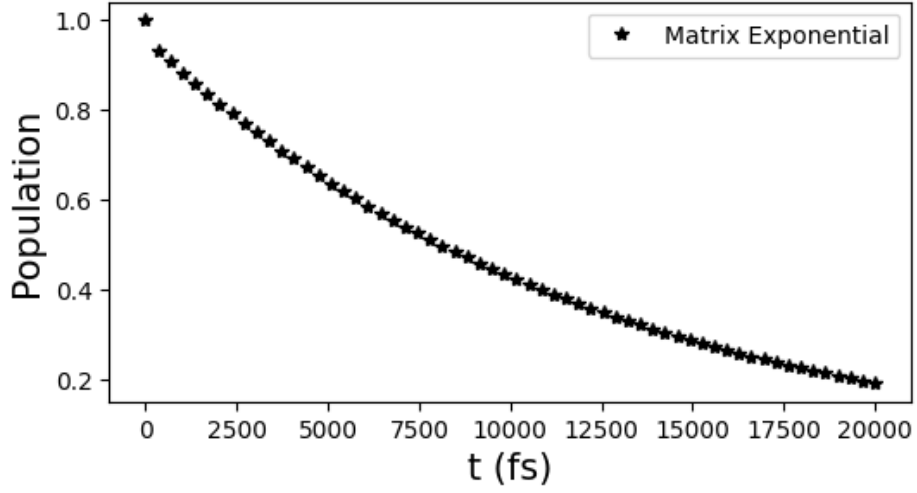
Figure 9: The long-time dynamics of the population in the right well for the double-well system. The result is obtained from matrix exponential propagation with the eigenstate truncation $N_{\text{eig}} = 30$.
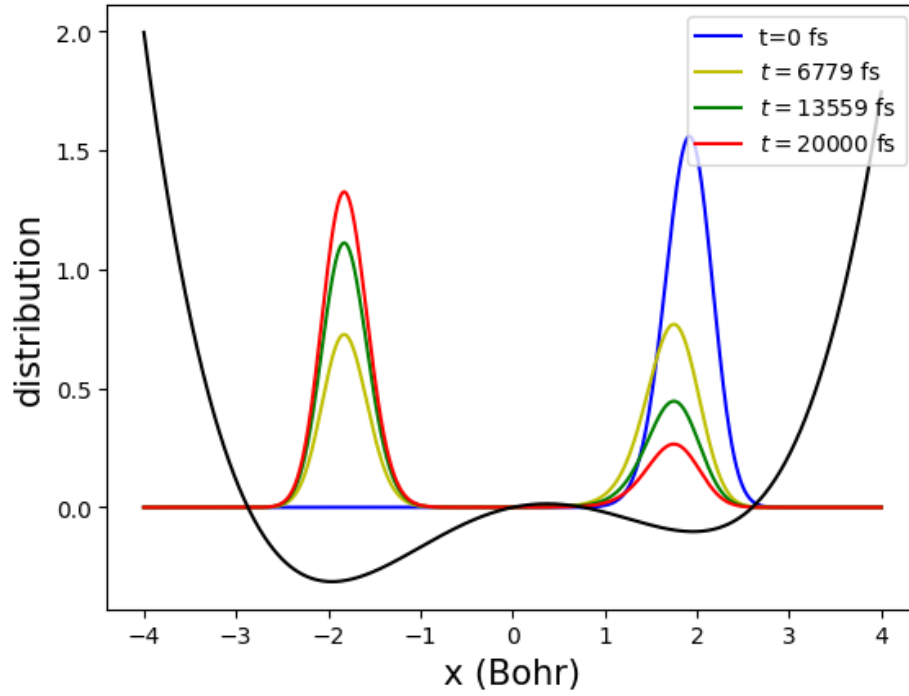

Figure 10: The proton probability density in the double-well potential at different time points.

6.2 Quantum Simulation

In this subsection, we use the dilation-based quantum algorithm to perform the quantum simulation of the Lindblad dynamics in the double-well Hamiltonian. The Hamiltonian and the corresponding Lindblad equation are the same as presented in Section 6.1. Here, we utilize the Kraus operator representation to evolve the system dynamics. Conceptually, each Kraus operator represents a distinct dissipative pathway contributing to the reduced dynamics of the proton.

This approach avoids the need to vectorize the density matrix (state vector of dimension N^2) and instead evolves a state vector in the system's N-dimensional Hilbert space. For cases where the density matrix has a high dimension, such as in the double-well model, this method significantly reduces the number of qubits required for the simulation.

In practice, within **QFlux**, the propagator obtained from the classical simulation is converted into Kraus operators, each of which is implemented as a separate quantum circuit. Script S.6.6 provides the **QFlux** package implementation for the quantum simulation of the Lindblad dynamics in the double-well potential. In this case, we extract the precomputed propagator from the classical simulation results in Section 6.1 ($N_{\text{eig}} = 30$). To match the qubit dimension, the `expand` function initializes the propagator to a $32^2 \times 32^2$ matrix. By creating a `DynamicsQ` object and specifying the Kraus operator representation, the **QFlux** package utilizes the technique from Section 2.1.3 to convert the propagator into Kraus operators and perform the quantum circuit simulation.

The quantum circuit simulation results shown in Fig. 11 are consistent with the results from the matrix exponential propagation, demonstrating the correctness of the quantum algorithm based on dilation and the Kraus operator representation.

In the following, we provide a detailed explanation of how the **QFlux** package implements this quantum simulation. First, Script S.6.7 presents the explicit definition for the `expand` function, which extends the propagator to match the qubit dimension. Then, Script S.6.8 converts the propagator into the Kraus operator representation.
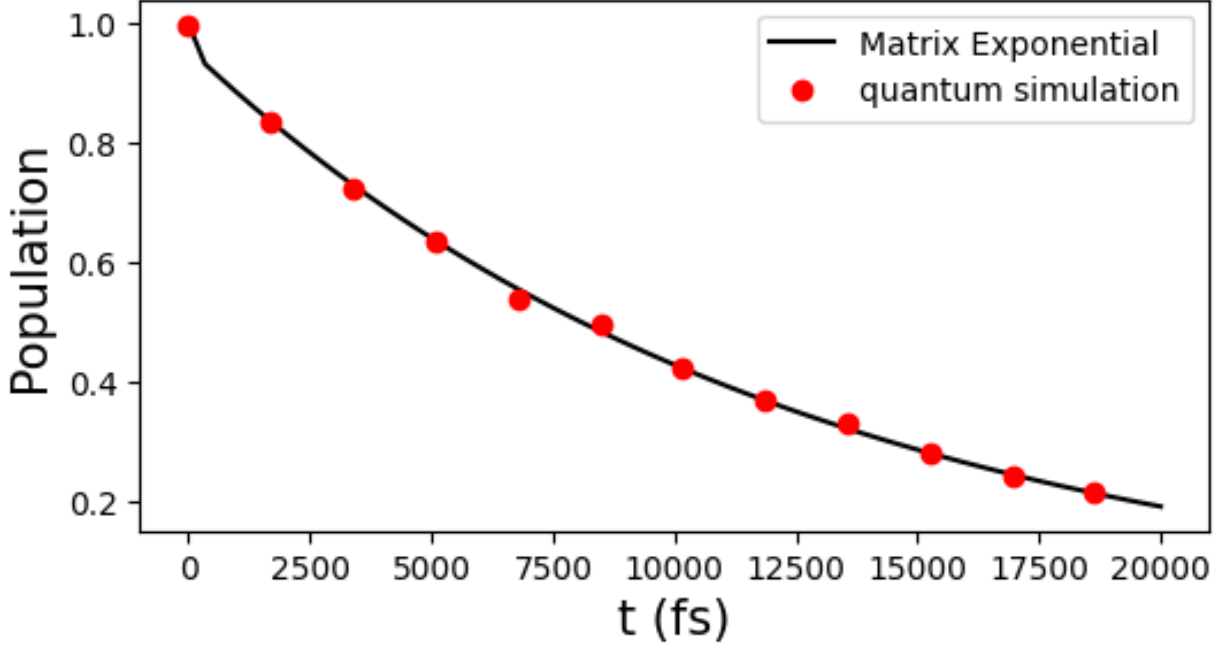
Figure 11: Quantum Aer simulation of the right well population dynamics in the double-well system. Each quantum circuit is measured with 2000 shots. The result is compared to the simulation from the matrix exponential propagation with the eigenstate truncation $N_{\mathrm{eig}} = 30$.

We compute the time evolution of the population in the right well through quantum simulations. Using the initial state from Eq. (6.4) and the Kraus representation from Eq. (2.3), the population $P_R(t)$ is expressed as

$$
\begin{aligned}
P_R(t) &= \mathrm{Tr}[\rho(t)\hat{P}_R] \\
&= \sum_i \mathrm{Tr}[M_i(t)|\psi(0)\rangle\langle\psi(0)|M_i^\dagger(t)\hat{P}_R] \\
&= \sum_i \langle\psi_i(t)|\hat{P}_R|\psi_i(t)\rangle \,,
\end{aligned}
\tag{6.10}
$$

where $\hat{P}_R$ is the Heaviside function $\Theta(x - x^*)$ [Eq. (6.5)] in the double-well eigenstate basis, and $|\psi_i(t)\rangle = M_i(t)|\psi(0)\rangle$. It should be noted that although the above equation uses the initial density matrix for the pure state $\rho(0) = |\psi(0)\rangle\langle\psi(0)|$, the form of the equation remains unchanged even if the initial density matrix corresponds to a mixed state. In such cases,

one only needs to include an index in the summation to iterate over the states of the initial mixed state.

The Kraus operators $M_i(t)$ are non-unitary and, by definition, they are always contraction mappings[38] satisfying the relation $\sum_i M_i M_i^\dagger \leq I$, with singular values bound above by 1, which makes the Sz.-Nagy dilation in Eq. (2.9) directly applicable without rescaling the matrix. After dilation, Eq. (6.10) acquires the form

$$P_R(t) = \sum_i \langle 0|\langle \psi(0)|U_{M_i}^\dagger \tilde{P}_R U_{M_i}|0\rangle|\psi(0)\rangle \tag{6.11}$$

where $|0\rangle$ is the state of the ancilla qubit, and the quantum circuit is initialized at $|0\rangle|\psi_0\rangle$, with $|\psi_0\rangle = |\phi_6\rangle$ as in Eq. (6.4). After applying the dilated Kraus operator U_{M_i} to the initial state, the result is obtained by measuring the expectation value of $\tilde{P}_R$ and summing over the indices of the Kraus operators. The operator $\tilde{P}_R$ in the dilated space is

$$\tilde{P}_R = \begin{bmatrix} \hat{P}_R & \mathbf{0} \\ \mathbf{0} & \mathbf{0} \end{bmatrix} . \tag{6.12}$$

It should be noted that the Kraus representation reduces the number of required qubits by nearly half compared to the vectorized density matrix representation. The trade-off is that each Kraus operator corresponds to a quantum circuit, meaning that the reduction in the number of qubits leads to an increase in the number of quantum circuits (up to N^2 quantum circuits may be needed).

To measure the observable $\tilde{P}_R$ on a quantum computer, it must be represented as the sum of the tensor products of the Pauli operators,

$$\tilde{P}_R = \sum_{\xi_1, \xi_2, \dots, \xi_n} a_{\xi_1 \xi_2 \cdots \xi_n} \, \xi_1 \xi_2 \cdots \xi_n \tag{6.13}$$

where each $\xi_i \in \left\{ I, \sigma^X, \sigma^Y, \sigma^Z \right\}$ is the Pauli operator operating on the i-th qubit and $a_{\xi_1 \xi_2 \cdots \xi_n}$

is a real number. The method for expressing a general Hermitian matrix in terms of the Pauli operators is demonstrated in **Part II** and is implemented here in the `ham_to_pauli` function. In Script S.6.9, we decompose $\tilde{P}_R$ with a given precision tol_p and convert it into a *Qiskit* operator.

The quantum simulation is performed in Script S.6.10, where we used `Estimator` function from `qiskit_aer.primitives` to use Aer implementation for measuring the expectation values of the observables after the execution of the quantum circuit. This yields the same results as the **QFlux** implementation in Script S.6.6.

7   Conclusions

In this tutorial, we have presented a comprehensive introduction to simulating the dynamics of open quantum systems on quantum computers. Throughout the discussion, we deliberately distinguished conceptual formulations of open-system dynamics from their realization in quantum circuits, enabling readers to engage with either the theoretical framework or the implementation details according to their interests.

We employed both vectorization of the density matrix and the Kraus operator representation to encode open-system states into qubit registers, and used the dilation method to construct quantum circuits capable of simulating non-unitary dynamics. By studying physically and chemically relevant models, we analyzed dissipative Lindblad dynamics and illustrated the role of environmental interactions in driving energy dissipation. In all cases, the quantum circuit simulations were found to be in good agreement with benchmarks obtained from classical computations, validating the correctness of the proposed approach.

In addition, this tutorial introduced the **QFlux** package, which provides a unified framework for simulating open-system dynamics on both classical and quantum platforms. The accompanying coding examples and detailed workflows are intended to help readers efficiently implement and adapt these methods to a wide range of problems in open quantum system

dynamics. Together, the methodology and software tools presented here lay the groundwork for future developments and applications in quantum simulations of dissipative systems.

Supporting Information

Detailed code snippets are available in the Supporting Information and corresponding Google Colab notebook as well as through the QFlux Documentation site.

Acknowledgements

References

(1) Hammes-Schiffer, S.; Soudackov, A. V. Proton-Coupled Electron Transfer in Solution, Proteins, and Electrochemistry. *Journal of Physical Chemistry B* **2008**, *112*, 14108–14123.

(2) Hammes-Schiffer, S.; Stuchebrukhov, A. A. Theory of Coupled Electron and Proton Transfer Reactions. *Chemical Reviews* **2010**, *110*, 6939–6960.

(3) Dan, X.; Xu, M.; Yan, Y.; Shi, Q. Generalized master equation for charge transport in a molecular junction: Exact memory kernels and their high order expansion. *Journal of Chemical Physics* **2022**, *156*, 134114.

(4) Dan, X.; Shi, Q. Theoretical study of nonadiabatic hydrogen atom scattering dynamics on metal surfaces using the hierarchical equations of motion method. *Journal of Chemical Physics* **2023**, *159*, 044101.

(5) Fenna, R. E.; Matthews, B. W. Chlorophyll arrangement in a bacteriochlorophyll protein from Chlorobium-Limicola. *Nature* **1975**, *258*, 573–577.

(6) Collini, E.; Wong, C. Y.; Wilk, K. E.; Curmi, P. M. G.; Brumer, P.; Scholes, G. D. Coherently wired light-harvesting in photosynthetic marine algae at ambient temperature. *Nature* **2010**, *463*, 644–647.

(7) Clarke, J.; Wilhelm, F. K. Superconducting quantum bits. *Nature* **2008**, *453*, 1031–1042.

(8) Büsser, C. A.; de Vega, I.; Heidrich-Meisner, F. Decoherence of an entangled state of a strongly correlated double quantum dot structure through tunneling processes. *Physical Review B* **2014**, *90*, 205118.

(9) Dan, X.; Xu, M.; Stockburger, J. T.; Ankerhold, J.; Shi, Q. Efficient low-temperature simulations for fermionic reservoirs with the hierarchical equations of motion method: Application to the Anderson impurity model. *Physical Review B* **2023**, *107*, 195429.

(10) de Vega, I.; Alonso, D. Dynamics of non-Markovian open quantum systems. *Reviews of Modern Physics* **2017**, *89*, 015001.

(11) Dan, X.; Long, Z.; Qiu, T.; Menzel, J. P.; Shi, Q.; Batista, V. Nonadiabatic H-Atom Scattering Channels on Ge (111) Elucidated by the Hierarchical Equations of Motion. *arXiv preprint arXiv:2509.16916* **2025**,

(12) Allen, B. C.; Batista, V. S.; Cabral, D. G. A.; Cianci, C.; Dan, X.; Dutta, R.; Geva, E.; Hu, Z.; Kais, S.; Khazaei, P.; Lyu, N.; Mulvihill, E.; Shivpuje, S.; Soudackov, A. V.;

Vu, N. P.; Wang, Y.; Wilson, C. QFlux — An Open-Source Python Package for Quantum Dynamics Simulations. https://qflux.batistalab.com, 2025; (accessed: 2025-10-12).

(13) Breuer, H.-P.; Petruccione, F. *The Theory of Open Quantum Systems*; Oxford University Press: New York, 2007.

(14) Nitzan, A. *Chemical Dynamics in Condensed Phases. Relaxation, Transfer, and Reactions in Condensed Molecular Systems*; Oxford University Press: New York, 2014.

(15) Manzano, D. A short introduction to the Lindblad master equation. *AIP Advances* **2020**, *10*, 025106.

(16) Borrelli, R.; Gelin, M. F. Finite temperature quantum dynamics of complex systems: Integrating thermo-field theories and tensor-train methods. *WIREs Computational Molecular Science* **2021**, *11*, e1539.

(17) Tanimura, Y. Numerically "Exact" Approach to Open Quantum Dynamics: The Hierarchical Equations of Motion (HEOM). *Journal of Chemical Physics* **2020**, *153*, 020901.

(18) Seneviratne, A.; Walters, P. L.; Wang, F. Exact Non-Markovian Quantum Dynamics on the NISQ Device Using Kraus Operators. *ACS Omega* **2024**, *9*, 9666–9675.

(19) Mulvihill, E.; Schubert, A.; Sun, X.; Dunietz, B. D.; Geva, E. A Modified Approach for Simulating Electronically Nonadiabatic Dynamics Via the Generalized Quantum Master Equation. *Journal of Chemical Physics* **2019**, *150*, 034101.

(20) Schlimgen, A. W.; Head-Marsden, K.; Sager, L. M.; Narang, P.; Mazziotti, D. A. Quantum simulation of the Lindblad equation using a unitary decomposition of operators. *Physical Review Research* **2022**, *4*, 023216.

(21) Dan, X.; Geva, E.; Batista, V. S. Simulating Non-Markovian Quantum Dynamics on

NISQ Computers Using the Hierarchical Equations of Motion. *Journal of Chemical Theory and Computation* **2025**, *21*, 1530–1546.

(22) Lindblad, G. On the Generators of Quantum Dynamical Semigroups. *Communications in Mathematical Physics* **1976**, *48*, 119–130.

(23) Gorini, V.; Kossakowski, A.; Sudarshan, E. C. G. Completely Positive Dynamical Semigroups of N-Level Systems. *Journal of Mathematical Physics* **1976**, *17*, 821–825.

(24) Schlimgen, A. W.; Head-Marsden, K.; Sager, L. M.; Narang, P.; Mazziotti, D. A. Quantum Simulation of Open Quantum Systems Using a Unitary Decomposition of Operators. *Physical Review Letters* **2021**, *127*, 270503.

(25) Li, X.; Lyu, S.-X.; Wang, Y.; Xu, R.-X.; Zheng, X.; Yan, Y. Toward quantum simulation of non-Markovian open quantum dynamics: A universal and compact theory. *Physical Review A* **2024**, *110*, 032620.

(26) Sweke, R.; Sinayskiy, I.; Bernard, D.; Petruccione, F. Universal simulation of Markovian open quantum systems. *Physical Review A* **2015**, *91*, 062308.

(27) Hu, Z.; Xia, R.; Kais, S. A quantum algorithm for evolving open quantum dynamics on quantum computing devices. *Scientific Reports* **2020**, *10*, 3301.

(28) Head-Marsden, K.; Krastanov, S.; Mazziotti, D. A.; Narang, P. Capturing non-Markovian dynamics on near-term quantum computers. *Physical Review Research* **2021**, *3*, 013182.

(29) Schlimgen, A. W.; Head-Marsden, K.; Sager-Smith, L. M.; Narang, P.; Mazziotti, D. A. Quantum state preparation and nonunitary evolution with diagonal operators. *Physical Review A* **2022**, *106*, 022414.

(30) Vu, N. P.; Dong, D.; Dan, X.; Lyu, N.; Batista, V.; Liu, Y. A Computational Framework for Simulations of Dissipative Nonadiabatic Dynamics on Hybrid Oscillator-Qubit Quantum Devices. *Journal of Chemical Theory and Computation* **2025**, *21*, 6258–6279.

(31) McArdle, S.; Jones, T.; Endo, S.; Li, Y.; Benjamin, S. C.; Yuan, X. Variational ansatz-based quantum simulation of imaginary time evolution. *npj Quantum Information* **2019**, *5*, 75.

(32) Motta, M.; Sun, C.; Tan, A. T. K.; O'Rourke, M. J.; Ye, E.; Minnich, A. J.; Brandao, F. G. S. L.; Chan, G. K.-L. Determining eigenstates and thermal states on a quantum computer using quantum imaginary time evolution. *Nature Physics* **2020**, *16*, 205–210.

(33) Kamakari, H.; Sun, S.-N.; Motta, M.; Minnich, A. J. Digital Quantum Simulation of Open Quantum Systems Using Quantum Imaginary–Time Evolution. *PRX Quantum* **2022**, *3*, 010320.

(34) Li, Y.; Benjamin, S. C. Efficient variational quantum simulator incorporating active error minimization. *Physical Review X* **2017**, *7*, 021050.

(35) Chen, M.-C.; Gong, M.; Xu, X.; Yuan, X.; Wang, J.-W.; Wang, C.; Ying, C.; Lin, J.; Xu, Y.; Wu, Y.; others Demonstration of adiabatic variational quantum computing with a superconducting quantum coprocessor. *Physical Review Letters* **2020**, *125*, 180501.

(36) Endo, S.; Sun, J.; Li, Y.; Benjamin, S. C.; Yuan, X. Variational Quantum Simulation of General Processes. *Physical Review Letters* **2020**, *125*, 010501.

(37) Lee, C.-K.; Hsieh, C.-Y.; Zhang, S.; Shi, L. Variational quantum simulation of chemical dynamics with quantum computers. *Journal of Chemical Theory and Computation* **2022**, *18*, 2105–2113.

(38) Nielsen, M. A.; Chuang, I. L. *Quantum computation and quantum information*; American Mathematical Society, 2010.

(39) Havel, T. F. Robust procedures for converting among Lindblad, Kraus and matrix representations of quantum dynamical semigroups. *Journal of Mathematical Physics* **2003**, *44*, 534–557.

(40) Choi, M.-D. Completely Positive Linear Maps on Complex Matrices. *Linear Algebra and Its Applications* **1975**, *10*, 285–290.

(41) Levy, E.; Shalit, O. M. Dilation theory in finite dimensions: the possible, the impossible and the unknown. *Rocky Mountain Journal of Mathematics* **2014**, *44*, 203–221.

(42) Wang, Y.; Mulvihill, E.; Hu, Z.; Lyu, N.; Shivpuje, S.; Liu, Y.; Soley, M. B.; Geva, E.; Batista, V. S.; Kais, S. Simulating Open Quantum System Dynamics on NISQ Computers with Generalized Quantum Master Equations. *Journal of Chemical Theory and Computation* **2023**, *19*, 4851–4862.

(43) Lyu, N.; Khazaei, P.; Geva, E.; Batista, V. S. Simulating Cavity-Modified Electron Transfer Dynamics on NISQ Computers. *Journal of Physical Chemistry Letters* **2024**, *15*, 9535–9542.

(44) Walters, P. L.; Wang, F. Path integral quantum algorithm for simulating non-Markovian quantum dynamics in open quantum systems. *Physical Review Research* **2024**, *6*, 013135.

(45) Welch, J.; Greenbaum, D.; Mostame, S.; Aspuru-Guzik, A. Efficient quantum circuits for diagonal unitaries without ancillas. *New Journal of Physics* **2014**, *16*, 033040.

(46) Carmichael, H. J. *Statistical Methods in Quantum Optics I: Master Equations and Fokker-Planck Equations*; Springer: Berlin, Heidelberg, 2013.

(47) Mohseni, M.; Rebentrost, P.; Lloyd, S.; Aspuru-Guzik, A. Environment-assisted quantum walks in photosynthetic energy transfer. *Journal of Chemical Physics* **2008**, *129*, 174106.

(48) Johansson, J. R.; Nation, P. D.; Nori, F. QuTiP: An open-source Python framework for the dynamics of open quantum systems. *Computer Physics Communications* **2012**, *183*, 1760–1772.

(49) Johansson, J. R.; Nation, P. D.; Nori, F. QuTiP 2: A Python framework for the dynamics of open quantum systems. *Computer Physics Communications* **2013**, *184*, 1234–1240.

(50) Wang, T.; Sanz, S.; Castro-Esteban, J.; Lawrence, J.; Berdonces-Layunta, A.; Mohammed, M. S. G.; Vilas-Varela, M.; Corso, M.; Peña, D.; Frederiksen, T.; de Oteyza, D. G. Magnetic Interactions Between Radical Pairs in Chiral Graphene Nanoribbons. *Nano Letters* **2022**, *22*, 164–171, PMID: 34936370.

(51) Fiori, E. R.; Pastawski, H. M. Non-Markovian decay beyond the Fermi Golden Rule: Survival collapse of the polarization in spin chains. *Chemical Physics Letters* **2006**, *420*, 35–41.

(52) Dong, H.; Zhang, P.; Dag, C. B.; Gao, Y.; Wang, N.; Deng, J.; Zhang, X.; Chen, J.; Xu, S.; Wang, K.; Wu, Y.; Zhang, C.; Jin, F.; Zhu, X.; Zhang, A.; Zou, Y.; Tan, Z.; Cui, Z.; Zhu, Z.; Shen, F.; Li, T.; Zhong, J.; Bao, Z.; Li, H.; Wang, Z.; Guo, Q.; Song, C.; Liu, F.; Chan, A.; Ying, L.; Wang, H. Measuring the Spectral Form Factor in Many-Body Chaotic and Localized Phases of Quantum Processors. *Physical Review Letters* **2025**, *134*.

(53) Javadi-Abhari, A.; Treinish, M.; Krsulich, K.; Wood, C. J.; Lishman, J.; Gacon, J.; Martiel, S.; Nation, P. D.; Bishop, L. S.; Cross, A. W.; Johnson, B. R.; Gambetta, J. M. Quantum computing with Qiskit. 2024; https://arxiv.org/abs/2405.08810.

(54) Godbeer, A. D.; Al-Khalili, J. S.; Stevenson, P. D. Modelling proton tunnelling in the adenine-thymine base pair. *Physical Chemistry Chemical Physics* **2015**, *17*, 13034–13044.

(55) Soley, M. B.; Bergold, P.; Gorodetsky, A. A.; Batista, V. S. Functional Tensor-Train Chebyshev Method for Multidimensional Quantum Dynamics Simulations. *Journal of Chemical Theory and Computation* **2021**, *18*, 25–36.

(56) Coffman, A. J.; Dou, W.; Hammes-Schiffer, S.; Subotnik, J. E. Modeling voltammetry curves for proton coupled electron transfer: The importance of nuclear quantum effects. *Journal of Chemical Physics* **2020**, *152*, 234108.

(57) Liu, X.; Dan, X.; Shi, Q. Theoretical study of proton-coupled electron transfer reaction in metal-hydride complexes. *Chin. J. Chem. Phys.* **2024**, *37*, 199–210.

(58) Shi, Q.; Zhu, L. L.; Chen, L. P. Quantum Rate Dynamics for Proton Transfer Reaction in a ModelSystem: Effect of the Rate Promoting Vibrational Mode. *Journal of Chemical Physics* **2011**, *135*, 044505.

(59) Xie, W.; Xu, Y.; Zhu, L.; Shi, Q. Mixed Quantum Classical Calculation of Proton Transfer Reaction Rates: From Deep Tunneling to over the Barrier Regimes. *Journal of Chemical Physics* **2014**, *140*, 174105.

(60) Cabral, D. G. A.; Khazaei, P.; Allen, B. C.; Videla, P. E.; Schäfer, M.; Cortiñas, R. G.; Carrillo de Albornoz, A. C.; Chávez-Carlos, J.; Santos, L. F.; Geva, E.; Batista, V. S. A Roadmap for Simulating Chemical Dynamics on a Parametrically Driven Bosonic Quantum Device. *Journal of Physical Chemistry Letters* **2024**, *15*, 12042–12050.

(61) de Albornoz, A. C. C.; Cortiñas, R. G.; Schäfer, M.; Frattini, N. E.; Allen, B.; Cabral, D. G. A.; Videla, P. E.; Khazaei, P.; Geva, E.; Batista, V. S.; Devoret, M. H. Oscillatory dissipative tunneling in an asymmetric double-well potential. 2024; https://arxiv.org/abs/2409.13113.

(62) Gautier, R.; Sarlette, A.; Mirrahimi, M. Combined Dissipative and Hamiltonian Confinement of Cat Qubits. *PRX Quantum* **2022**, *3*, 020339.

(63) Venkatraman, J.; Cortinas, R. G.; Frattini, N. E.; Xiao, X.; Devoret, M. H. A driven quantum superconducting circuit with multiple tunable degeneracies. 2023; https://arxiv.org/abs/2211.04605.

Supporting Information for

QFlux: An Open-Source Toolkit for Quantum Dynamics Simulations on Quantum Computers.

Part IV – Dilation Method for Open Quantum Systems

Xiaohan Dan,[†] Saurabh Shivpuje,[‡] Yuchen Wang,[‡] Delmar G. A. Cabral,[†] Brandon C. Allen,[†] Pouya Khazaei,[¶] Alexander V. Soudackov,[†] Zixuan Hu,[‡] Ningyi Lyu,[†] Eitan Geva,[¶] Sabre Kais,[*,§] and Victor S. Batista[*,†]

[†]*Department of Chemistry, Yale Quantum Institute, Yale University, New Haven, CT 06511, USA*

[‡]*Department of Chemistry, Purdue University, West Lafayette, Indiana 47907, USA*

[¶]*Department of Chemistry, University of Michigan, Ann Arbor, MI 48109, USA*

[§]*Department of Electrical and Computer Engineering, Department of Chemistry, North Carolina State University, Raleigh, North Carolina 27606, USA*

E-mail: skais@ncsu.edu; victor.batista@yale.edu

Contents

S.1 From Propagators to Kraus Maps

We begin by converting a superoperator (propagator) $G(t)$ acting on the vectorized density matrix into an operator-sum (Kraus) representation $\mathcal{E}_t(\rho) = \sum_i M_i(t)\rho M_i^\dagger(t)$. This proceeds by building the Choi matrix of $G(t)$ and diagonalizing it; eigenvectors yield Kraus operators. The routine below implements that construction with a tolerance to drop numerically negligible modes.

Script S.1.1: Obtaining Kraus operators from the propagator

```python
import numpy as np
import scipy.linalg as LA

def gen_Kraus_list(Gmat,N,tol=1E-5):
    """
    Generate the Kraus operators from the propagator with a given tolerance
    Input:
    - Gmat: matrix of the propagator (numpy array of shape (N^2, N^2)).
    - N: The system Hilbert space dimension
    - tol: tolerance for the Kraus operator representation.
    Returns:
    - Kraus: List of Kraus operators
    """
    # defining the Choi matrix from the matrix of the propagator
    C_mat = np.zeros(Gmat.shape,dtype=np.complex128)
    for i in range(N):
        for j in range(N):
            C_matij = np.zeros(Gmat.shape,dtype=np.complex128)
            for k in range(N):
                for l in range(N):
                    C_matij[i*N+k,l*N+j] = Gmat[j*N+k,l*N+i]
            C_mat += C_matij

    Kraus = []
    val,arr = LA.eigh(C_mat)
    for i in range(len(val)):
        if (val[i]>tol):
            Mi = np.sqrt(val[i])*arr[:,i].reshape(N,N)
            Kraus.append(Mi.conj().T)
    return Kraus
```

S.2 Unitary Dilations for Quantum Simulation

Open-system maps can be embedded into larger unitary evolutions via Sz.-Nagy (or SVD-based) dilation. The routine below constructs a $2N \times 2N$ unitary $\mathcal{U}$ whose action on an enlarged space reproduces the original contraction after tracing out ancillas. Optional scaling ensures the contraction property when the input matrix is not strictly contractive.

Script S.2.1: Dilation

```python
def dilate(array,Isscale=True):

    if(Isscale):
        # Normalization factor, 1.1 times martix's norm to ensure contraction
        norm = LA.norm(array,2)*1.1
        array_new = array/norm
    else:
        array_new = array

    ident = np.eye(array.shape[0])

    # Calculate the conjugate transpose of the G propagator
    fcon = (array_new.conjugate()).T

    # Calculate the defect matrix for dilation
    fdef = LA.sqrtm(ident - np.dot(fcon, array_new))

    # Calculate the defect matrix for the conjugate of the G propagator
    fcondef = LA.sqrtm(ident - np.dot(array_new, fcon))

    # Dilate the G propagator to create a unitary operator
    array_dilated = np.block([[array_new, fcondef], [fdef, -fcon]])
    if(Isscale):
        return array_dilated, norm
    else:
        return array_dilated
```

S.3 Lindblad Dynamics

We now assemble tools to compute dynamics governed by the Lindblad master equation. The generator acts linearly on the vectorized density matrix, enabling propagation via a matrix exponential.

S.3.1 Propagator via Matrix Exponential

Script S.3.1: Calculating the propagator of the Lindblad equation

```python
def Gt_matrix_expo(H, L, time_arr, Is_show_step = False):
    """
    Getting the propagator of the Lindblad equation by matrix exponential
    Parameters:
    - H: Hamiltonian of the system (numpy array of shape (N, N)).
    - time_arr: Time array for dynamic simulation (array).
    - L: List of Collapse operators, with each operator is a numpy array of shape (N,
     N).
    Returns:
    - G_prop: List of propagators.
    """
    Nsys = H.shape[0]
    ident_h = np.eye(Nsys, dtype=np.complex128)

    # Amatrix for time-derivation of the vectorized density matrix
    Amat = -1j * (np.kron(H, ident_h) - np.kron(ident_h, H.T))
    for i in range(len(L)):
        Amat += 0.5 * (2.0 * (np.kron(L[i], L[i].conj()))
                       - np.kron(ident_h, L[i].T @ L[i].conj())
                       - np.kron(L[i].T.conj() @ L[i], ident_h))

    G_prop = []
    for i in range(len(time_arr)):
        if(Is_show_step): print('step',i,'time',time_arr[i])
        Gt = LA.expm(Amat * time_arr[i])
        G_prop.append(Gt)
    return G_prop
```

S.3.2 Direct Time Evolution and Observables

The helper below wraps propagation and evaluation of an observable $\langle O(t) \rangle = \text{Tr}[\rho(t)O]$. Optional flags store full states and/or return the propagators for reuse.

Script S.3.2: Solving the Lindblad equation via matrix exponential

```python
def propagate_matrix_exp(H, rho0, time_arr, L, observable, Is_store_state = False,
    Is_show_step = False, Is_Gt = False):
    """
    Solving the Lindblad equation by matrix exponential
    Parameters:
    - H: Hamiltonian of the system (numpy array of shape (N, N)).
    - rho0: Initial density matrix (numpy array of shape (N, N)).
    - time_arr: Time array for dynamic simulation (array).
    - L: List of Collapse operators, with each operator is a numpy array of shape (N,
     N).
    - observable: Observable for which the expectation value is computed (numpy array
     of shape (N, N)).
    - Is_store_state: Boolean variable that determines whether to output the density
     matrix list
    - show_step: Boolean variable that determines whether to print the current step
     during simulation
    Returns:
    - result: A class containing all the results
      result.expect: List of expectation values of the observable over time.
      result.G_prop: List of propagators.
      result.density_matrix: List of density matrices.
    """

    class Result:
        def __init__(self):
            self.expect = []
            if(Is_store_state):
                self.density_matrix = []
            if(Is_Gt):  self.Gprop = None
    result = Result()

    # Getting the propagator of the Lindblad equation
    G_prop = Gt_matrix_expo(H, L, time_arr, Is_show_step)
    if(Is_Gt):  result.Gprop = G_prop

    # initialized vectorized density matrix
    Nsys = H.shape[0]
```

```
    vec_rho0 = rho0.reshape(Nsys**2)

    for i in range(len(time_arr)):

        vec_rhot = G_prop[i] @ vec_rho0

        # get the density matrix by reshaping
        rhot = vec_rhot.reshape(Nsys, Nsys)

        if(Is_store_state):  result.density_matrix.append(rhot)
        result.expect.append(np.trace(rhot @ observable).real)

    return result
```

S.3.3 Benchmarking Against QuTiP

For validation we compare with `mesolve` from QuTiP, using identical Hamiltonians and collapse operators.

Script S.3.3: QuTiP for Exact Solutions 🔗

```python
from qutip import mesolve, Qobj

def qutip_prop(H, rho0, time_arr, c_ops, observable):
    """
    First import the mesolve function, which is used to solve master equations, and
     the Qobj class, which is used to represent quantum objects, from the QuTiP
     library.
    - H: Hamiltonian of the system (Qobj).
    - rho0: Initial density matrix (Qobj).
    - time_arr: Time array for dynamic simulation (array).
    - c_ops: List of collapse operators (list of Qobj), can be empty for Liouville
     equation.
    - observable: Operator for which the expectation value is to be calculated (Qobj).
    Returns:
    - expec_vals: List of expectation values of the observable over time.
    """
    result = mesolve(H, rho0, time_arr, c_ops=c_ops, e_ops=observable)
    return result.expect
```

S.4 Example: Single Qubit (Spin-$\frac{1}{2}$)

We illustrate the workflow on a driven-dissipative qubit with $H = 2\pi \cdot 0.1\, \sigma_x$ and collapse $L = \sqrt{\gamma}\, \sigma_x$.

S.4.1 System Setup

Script S.4.1: Set up the Spin-1/2 system

```python
from qflux.open_systems import params as pa

# The Spin-1/2 system Hamiltonian
H_1spin = 2 * np.pi * 0.1 * pa.X

# The jump operator and damping rate of Spin-1/2 system
gamma_1spin = 0.05
L_1spin = np.sqrt(gamma_1spin)*pa.X

# Initial density matrix
rho0_1spin = np.outer(pa.spin_up, pa.spin_up.conj())

# Time array for simulation
time_arr = np.linspace(0, (250 - 1) * 0.1, 250)
```

S.4.2 Propagation and Benchmarks

Script S.4.2: Propagate the Spin-1/2 system

```python
# Matrix Exponential Propagation
result_matrix_exp = propagate_matrix_exp(H_1spin, rho0_1spin, time_arr, [L_1spin],
    pa.Z)
```

```
# QuTiP Propagation for Liouville equation (no collapse operator)
expec_vals_qutip_Liouv = qutip_prop(Qobj(H_1spin), Qobj(rho0_1spin), time_arr, [],
    Qobj(pa.Z))

# QuTiP Propagation for Lindblad equation
expec_vals_qutip_Lindblad = qutip_prop(Qobj(H_1spin), Qobj(rho0_1spin), time_arr,
    [Qobj(L_1spin)], Qobj(pa.Z))
```

S.4.3 Visualization

Script S.4.3: Plot the results: Spin 1/2 system 🔗

```python
import matplotlib.pyplot as plt
plt.figure(figsize=(6,4))
plt.plot(time_arr, result_matrix_exp.expect,'b-', label = "Matrix Exponential")
plt.plot(time_arr, expec_vals_qutip_Lindblad[0],'ko',markersize=4,markevery=4,
    label = "QuTiP_Lindblad")
plt.plot(time_arr, expec_vals_qutip_Liouv[0],'r-', label = "QuTiP_Liouville")
plt.xlabel('time',fontsize=15)
plt.ylabel(r'$\langle\sigma^z\rangle (t)$',fontsize=15)
plt.ylim(-1.1,1.8)
plt.legend(loc = 'upper right')
plt.show()
```

S.4.4 High-Level QFlux Interfaces

The same computation can be scripted through **QFlux** abstractions, which encapsulate Hamiltonians, collapse sets, and propagation options.

```python
from qflux.open_systems import params as pa
from qflux.open_systems.numerical_methods import DynamicsOS
from qflux.open_systems.quantum_simulation import QubitDynamicsOS
import numpy as np

# Classical Simulation
# set the Hamiltonian and initial state
# The Spin-1/2 system Hamiltonian
Hsys = 2 * np.pi * 0.1 * pa.X

# The collapse operator and damping rate of Spin-1/2 system
gamma = 0.05
c_ops = np.sqrt(gamma)*pa.X

# Initial density matrix
rho0 = np.outer(pa.spin_up, pa.spin_up.conj())

# Time array for simulation
time_arr = np.linspace(0, (250 - 1) * 0.1, 250)

# instantiation
spin1_puresys = DynamicsOS(Nsys=2, Hsys=Hsys, rho0=rho0)
spin1_dissipative = DynamicsOS(Nsys=2, Hsys=Hsys, rho0=rho0, c_ops = [c_ops])

# propagation
# QuTiP Propagation for the pure system Liouville equation (for comparison)
expec_vals_qutip_Liouv = spin1_puresys.propagate_qt(time_arr=time_arr,
    observable=pa.Z)

# matrix exponential propagation
result_matrix_exp = spin1_dissipative.propagate_matrix_exp(time_arr=time_arr,
    observable=pa.Z)

# QuTiP Propagation for the Lindblad equation
expec_vals_qutip_Lindblad = spin1_dissipative.propagate_qt(time_arr=time_arr,
    observable=pa.Z)
```

S.4.5   Amplitude Damping on a Qubit

We next simulate an amplitude-damping channel both classically and via dilated unitaries on a quantum backend, enabling a one-to-one comparison.

Script S.4.5: Quantum Simulation of Amplitude Damping with QFlux

```python
import numpy as np

# Quantum Simulation: Amplitude damping channel
# System Hamiltonian
Hsys = 0.0 * pa.I

# The collapse operator and damping rate
gamma = 1.52e9*1E-12 # the spontaneous emission rate, ps^-1
c_ops = np.sqrt(gamma)*pa.sigmap

# Initial density matrix
rho0_sdam = np.array([[1/4,1/4],[1/4,3/4]],dtype=np.complex128)


time_sdam = np.arange(0, 1000, 1) #time array, from t=0 to t=1000 ps

# instantiation
spin1_sdam = QubitDynamicsOS(rep='Density', Nsys=2, Hsys=Hsys, rho0=rho0_sdam,
    c_ops = [c_ops])
# set qubit state to measurement
spin1_sdam.set_count_str(['000','011'])
# set the dilation method, which can be 'Sz-Nagy' or 'SVD' or 'SVD-Walsh'
spin1_sdam.set_dilation_method('SVD')

# quantum simulation
Pop_qc = spin1_sdam.qc_simulation_vecdens(time_sdam)

# compare to classical
res_sdam_classical = spin1_sdam.propagate_matrix_exp(time_sdam, observable=pa.Z,
    Is_store_state = True)

Pop_Mexp = np.zeros_like(Pop_qc['data'])
for i in range(len(time_sdam)):
    Pop_Mexp[i,0] = res_sdam_classical.density_matrix[i][0,0].real
    Pop_Mexp[i,1] = res_sdam_classical.density_matrix[i][1,1].real
```

S.4.6 Population Dynamics

```python
plt.figure(figsize=(6,4))
plt.plot(time_sdam,Pop_qc['data'][:,0],'r-',label=r"quantum, $|0\rangle$")
plt.plot(time_sdam,Pop_Mexp[:,0],'ko',markersize=5,markevery=40,label=r"benchmark,
    $|0\rangle$")
plt.plot(time_sdam,Pop_qc['data'][:,1],'b-',label=r"quantum, $|1\rangle$")
plt.plot(time_sdam,Pop_Mexp[:,1],'yo',markersize=5,markevery=40,label=r"benchmark,
    $|1\rangle$")
plt.xlabel('time (ps)',fontsize=15)
plt.ylabel('$P(t)$',fontsize=15)
plt.legend(loc = 'center right')
plt.show()
```

S.4.7 Propagator and Quantum-Circuit Realization

We explicitly form $G(t)$ for the amplitude-damping channel, evolve the state classically, and then embed each $G(t)$ into a circuit via dilation to compare shot-based estimates.

Script S.4.7: Amplitude Damping Channel: Propagator 🔗

```python
gamma = 1.52e9*1E-12 # the spontaneous emission rate, ps^-1
time_sdam = np.arange(0, 1000, 1) # time array, from t=0 to t=1000 ps
Nsys_1spin = 2

# defining the initial density matrix rho
rho0_sdam = np.array([[1/4,1/4],[1/4,3/4]],dtype=np.complex128)
vec0_sdam = rho0_sdam.reshape(Nsys_1spin**2)
norm0_sdam = LA.norm(vec0_sdam,2)
vec0_sdam /= norm0_sdam

Pop_Mexp = np.zeros((len(time_sdam),2),dtype=np.float64) #population array

Gprop_sdam = Gt_matrix_expo(0.0*pa.X, [np.sqrt(gamma)*pa.sigmap], time_sdam)

for i in range(len(time_sdam)):

    Gt = Gprop_sdam[i]
    rhot_sdam = (Gt@vec0_sdam).reshape(Nsys_1spin,Nsys_1spin)*norm0_sdam
    Pop_Mexp[i,0] = rhot_sdam[0,0].real
```

```
        Pop_Mexp[i,1] = rhot_sdam[1,1].real
```

S.5 Example: Open Spin Chain

We extend to a three-site spin chain with local fields and nearest-neighbor XYZ couplings.
The initial state is $|\uparrow\downarrow\downarrow\rangle$ and we monitor a survival amplitude observable.

S.5.1 Parameters and Initial State

Script S.5.1: Spin Chain Parameter and initial state 🔗

```python
# the system Hamiltonian parameter
nsite = 3 #this states how many spins in the simulation
Nsys_sc = 2**nsite #this is the dimension of the Hilbert space
Omegai_list = [0.65, 1.0, 1.0]
Jix_list = [0.75, 1.0]
Jiy_list = [0.75, 1.0]
Jiz_list = [0.0, 0.0]

# set up the initial state at [up,down,down...]
init_state = pa.spin_up
for i in range(nsite-1):
    init_state = np.kron(init_state,pa.spin_down)

# set up the initial density matrix according to initial state
rho0_sc = np.zeros((Nsys_sc,Nsys_sc),dtype=np.complex128)
rho0_sc += np.outer(init_state,init_state.conj())

# time array for simulation
nsteps = 250
time_arr = np.linspace(0, (nsteps - 1) * 0.1, nsteps)
```

S.5.2 Hamiltonian Construction

```python
# the diagonal part of the Hamiltonian
H_diag = np.zeros((Nsys_sc,Nsys_sc),dtype=np.complex128)
for n in range(nsite):
    tmp = 1.0
    for i in range(nsite):
        if(i==n):
            tmp = np.kron(tmp,pa.Z)
        else:
            tmp = np.kron(tmp,pa.I)
    H_diag += Omegai_list[n]*tmp

# the non-diagnoal (coupling) part of the Hamiltonian
H_coup = np.zeros((Nsys_sc,Nsys_sc),dtype=np.complex128)
XX = np.kron(pa.X,pa.X)
YY = np.kron(pa.Y,pa.Y)
ZZ = np.kron(pa.Z,pa.Z)
for n in range(nsite-1):
    coup_tmp = Jix_list[n]*XX+Jiy_list[n]*YY+Jiz_list[n]*ZZ
    tmp = 1.0
    for i in range(nsite-1):
        if(n==i):
            tmp = np.kron(tmp,coup_tmp)
        else:
            tmp = np.kron(tmp,pa.I)
    H_coup += tmp
Hsys_sc = H_diag - 0.5 * H_coup
Hsys_sc_qobj = Qobj(Hsys_sc)
```

S.5.3 Dissipation Model

```python
# The lindblad damping rate
Gamma1 = [0.016]*nsite
Gamma2 = [0.0523]*nsite

# The Collapse operators
L_sc = []
L_sc_qobj = [] #this stores Qobj type for QuTiP methods
```

```python
sigma2 = pa.sigmap@pa.sigmam

for isite in range(nsite):
    # Lindbladian for type 1
    res = 1.0
    for j in range(nsite):
        if(j==isite):
            res = np.kron(res,pa.sigmam)*np.sqrt(Gamma1[isite])
        else:
            res = np.kron(res,pa.I)
    L_sc.append(res)
    L_sc_qobj.append(Qobj(res))

    # Lindbladian for type 2
    res = 1.0
    for j in range(nsite):
        if(j==isite):
            res = np.kron(res,sigma2)*np.sqrt(Gamma2[isite])
        else:
            res = np.kron(res,pa.I)
    L_sc.append(res)
    L_sc_qobj.append(Qobj(res))
```

S.5.4 Classical Dynamics and Benchmarks

Script S.5.4: Spin Chain Dynamics 🔗

```python
# Matrix Exponential Propagation
result_matrix_exp = propagate_matrix_exp(Hsys_sc, rho0_sc, time_arr, L_sc, rho0_sc)

rho0_sc_qobj = Qobj(rho0_sc)
# QuTiP Propagation for Liouville equation (no collapse operator)
result_qutip_Liouv = qutip_prop(Hsys_sc_qobj, rho0_sc_qobj, time_arr, [],
    rho0_sc_qobj)

# QuTiP Propagation for Lindblad equation
result_qutip_Lindblad = qutip_prop(Hsys_sc_qobj, rho0_sc_qobj, time_arr,
    L_sc_qobj, rho0_sc_qobj)

As_matrix_exp = np.sqrt(result_matrix_exp.expect[:])
```

```
As_qutip = np.sqrt(result_qutip_Lindblad[0][:])
As_qutip_liouv = np.sqrt(result_qutip_Liouv[0][:])
```

S.5.5   Visualization

Script S.5.5: Plot the results: Spin Chain 🔗

```python
plt.figure(figsize=(6,4))
plt.plot(time_arr,As_matrix_exp,'b-', label="Matrix Exponential")
plt.plot(time_arr,As_qutip,'ko',markersize=4,markevery=4,label="QuTiP_Lindblad")
plt.plot(time_arr,As_qutip_liouv,'r-',label="Pure System")
plt.xlabel('time',fontsize=15)
plt.ylabel('$A_s(t)$',fontsize=15)
plt.ylim(0,1.35)
plt.legend(loc = 'upper right')
plt.show()
```

S.5.6   High-Level QFlux API (Classical)

Script S.5.6: Simulating Spin Chain Dynamics with QFlux 🔗

```python
from qflux.open_systems import DynamicsOS

# Classical Simulation
# instantiation
spin_chain_puresys = DynamicsOS(Nsys=Nsys_sc, Hsys=Hsys_sc, rho0=rho0_sc)
spin_chain_opensys = DynamicsOS(Nsys=Nsys_sc, Hsys=Hsys_sc, rho0=rho0_sc, c_ops =
    L_sc)

# propagation
# QuTiP Propagation for the pure system Liouville equation (for comparison)
```

```
result_qutip_Liouv = spin_chain_puresys.propagate_qt(time_arr=time_arr,
    observable=rho0_sc)

# matrix exponential propagation
result_matrix_exp = spin_chain_opensys.propagate_matrix_exp(time_arr=time_arr,
    observable=rho0_sc)

# QuTiP Propagation for the Lindblad equation
result_qutip_Lindblad = spin_chain_opensys.propagate_qt(time_arr=time_arr,
    observable=rho0_sc)

As_matrix_exp = np.sqrt(result_matrix_exp.expect[:])
As_qutip = np.sqrt(result_qutip_Lindblad[0][:])
As_qutip_liouv = np.sqrt(result_qutip_Liouv[0][:])
```

S.5.7   Quantum Simulation with QFlux

We next recast the open-system evolution in terms of unitary circuits with an ancillary qubit
and evaluate observables by sampling measurement outcomes.

Script S.5.7: Quantum Simulation of Spin Chain with QFlux

```python
from qflux.open_systems import QubitDynamicsOS

# Quantum Simulation
qspin_chain = QubitDynamicsOS(rep='Density',Nsys=Nsys_sc, Hsys=Hsys_sc,
    rho0=rho0_sc, c_ops = L_sc)
qspin_chain.set_count_str(['0011011'])

res_qc_1k = qspin_chain.qc_simulation_vecdens(time_arr,shots=1000)
res_qc_1w = qspin_chain.qc_simulation_vecdens(time_arr,shots=10000)

As_qc_1k = np.sqrt(res_qc_1k['data'])
As_qc_1w = np.sqrt(res_qc_1w['data'])
```

Script S.5.8: Plot the Quantum Result of Spin Chain 🔗 🐍

```python
plt.figure(figsize=(6,2))
plt.plot(time_arr,As_qc_1k[:],'r-',label=f"quantum,counts={1000}")
plt.plot(time_arr,As_qc_1w[:],'b-',label=f"quantum,counts={10000}")
plt.plot(time_arr,As_qutip,'ko',markersize=4,markevery=4,label="QuTiP benchmark")
plt.xlabel('Time',fontsize=15)
plt.ylabel('$A_s$(t)',fontsize=15)
plt.legend(loc = 'upper right')
```

S.5.8 Low-Level Circuit Realization

The next block shows a manual circuit construction using the explicit dilated propagator at each time step.

Script S.5.9: Quantum Simulation of Spin Chain 🔗 🐍

```python
# initial state of the spin chain in the dilated space
# rho0_sc=|up,down,...><up,down,...|, has defined in the Digital computer
    simulation part
rho0_sc_dil = np.concatenate((rho0_sc.reshape(Nsys_sc**2),np.zeros(Nsys_sc**2)))

# The propagator of the spin chain Lindblad equation
Gprop_sc = Gt_matrix_expo(Hsys_sc, L_sc, time_arr)

aersim=AerSimulator()
shots_arr = [1000,10000]
As_qc_1k = np.zeros((nsteps),dtype=np.float64)
As_qc_1w = np.zeros((nsteps),dtype=np.float64)
As_qc = [As_qc_1k,As_qc_1w]
nsteps = len(time_arr)

for i in range(nsteps):
    if(i%10==0):print('istep',i)
    qr = QuantumRegister(nsite*2+1)  # Create a quantum register
    cr = ClassicalRegister(nsite*2+1)  # Create a classical register to store
     measurement results
    qc = QuantumCircuit(qr, cr)  # Combine the quantum and classical registers to
     create the quantum circuit
```

```
    # Initialize the quantum circuit with the initial state
    qc.initialize(rho0_sc_dil, qr)
    # Dilated propagator
    U_G, norm = dilate(Gprop_sc[i])

    # Create a custom unitary operator with the dilated propagator
    U_G_op = Operator(U_G)

    # Apply the unitary operator to the quantum circuit's qubits
    qc.unitary(U_G_op, qr)

    qc.measure(qr, cr)

    for ishot in range(len(shots_arr)):
        counts1 = aersim.run(qc,shots=shots_arr[ishot]).result().get_counts()
        if '0011011' in counts1:
            survi_amp = np.sqrt(counts1['0011011']/shots_arr[ishot])*norm
            As_qc[ishot][i] = np.sqrt(survi_amp)
        else:
            print(i,'shots=',shots_arr[ishot],"no counts")
```

S.6 Example: Double-Well Potential

Finally, we treat a dissipative vibrational system in a double-well potential. We discretize in real space, build eigenstates, and move to a truncated eigenbasis for efficient open-system simulation.

S.6.1 Potential and Discretization

Script S.6.1: Double-Well potential ↗

```
def pot_doublewell(x, f=0.0367493, a0=0.0, a1=0.429, a2=-1.126, a3=-0.143,
    a4=0.563):
    # A-T pair double-well potential in Hartrees (x is in Bohr)
    xi = x/1.9592
    return f*(a0 + a1*xi + a2*xi**2 + a3*xi**3 + a4*xi**4)
```

```
# The parameters
# Note that some unit conversion constants are defined in the pa object (an
    implementation of the Params class)
mass0 = 1836.15
beta = pa.au2joule/(pa.bolz*300) #1/(kT) in a.u. units
omega = 0.00436 #the frequency associate with the right well
kappa = 1/(10/pa.au2fs)
nth = 1/(np.exp(beta*omega)-1)

# set up the grid point
xmin = -4.0
xmax = 4.0
ndvr = 1024
xgrid = np.linspace(xmin,xmax,ndvr)

pot_arr = pot_doublewell(xgrid)

plt.plot(xgrid,pot_arr,'k', label = "V(x)")
plt.xlabel('$x$ (Bohr)',fontsize=15)
plt.ylabel('$V(x)$ (a.u.)',fontsize=15)
plt.ylim(-0.04,0.1)
plt.legend(loc = 'upper center')
plt.show()
```

S.6.2   Eigenstates and Basis Truncation

Script S.6.2: Eigenstates in the Double-well Potential 🔗

```python
import scipy.fft as sfft

def get_eig_state(hamk,pot,xgrid,Nstate):
    """
    get the eigen state for potential in x-space
    input:kinetic energy hamiltonian, potential in x-space
    """
    Mata = hamk.copy()
    for i in range(ndvr):
        Mata[i,i]+=pot[i]

    val,arr = LA.eigh(Mata)
```

```python
    dx = xgrid[1]-xgrid[0]
    return val[:Nstate],arr[:,:Nstate]/dx**0.5

kgrid = np.zeros(ndvr,dtype=np.float64)
# ak2: kinetic energy array in k-space
ak2   = np.zeros(ndvr,dtype=np.float64)

dx = xgrid[1]-xgrid[0]
dk = 2.0*np.pi/((ndvr)*dx)
coef_k = pa.hbar**2/(2.0*mass0)

for i in range(ndvr):
  if(i<ndvr//2):
    kgrid[i] = i*dk
  else:
    kgrid[i] = -(ndvr-i) * dk

  ak2[i] = coef_k*kgrid[i]**2

akx0 = sfft.ifft(ak2)
# hamk: kinetic hamiltonian Matrix in position x grid space
hamk = np.zeros((ndvr,ndvr),dtype=np.complex128)

for i in range(ndvr):
  for j in range(ndvr):
    if(i<j):
      hamk[i,j] = akx0[i-j].conj()
    else:
      hamk[i,j] = akx0[i-j]

Neig = 50
eneg_DW,psi_DW = get_eig_state(hamk,pot_arr,xgrid,Neig)
```

S.6.3 Operators in the Eigenbasis

We express x, p, ladder operators, and left/right well projectors in the truncated eigenbasis, and choose a localized initial state.

Script S.6.3: Express operators in terms of eigenstate basis 🔗 🐍

```python
# the eigenstate in the k-space representation
# ( by Fourier transform of the original eigenstate in x-space)
psik_DW = np.zeros((ndvr,Neig),dtype=np.complex128)
pre_fac = dx/(2*np.pi)**0.5
for i in range(Neig):
    psik_DW[:,i] = sfft.fft(psi_DW[:,i])*pre_fac

# initial density matrix
ini_occu = np.zeros(Neig,dtype=np.complex128)
ini_occu[5] = 1.0
rho0 = np.outer(ini_occu,ini_occu.conj())

# The operator in the eigenstate
xmat_eig = np.zeros((Neig,Neig),dtype=np.complex128)
pmat_eig = np.zeros((Neig,Neig),dtype=np.complex128)
for i in range(Neig):
    for j in range(Neig):
        xmat_eig[i,j] = np.dot(np.multiply(psi_DW[:,i].conj(),xgrid),psi_DW[:,j])*dx
        pmat_eig[i,j] =
    np.dot(np.multiply(psik_DW[:,i].conj(),kgrid),psik_DW[:,j])*dk

# hamiltonian
H_dw = np.diag(eneg_DW)
# creation/annihilation operator
amat_eig =
    xmat_eig.copy()*np.sqrt(mass0*omega/2)+1j*pmat_eig.copy()/np.sqrt(mass0*omega*2)
adegmat_eig =
    xmat_eig.copy()*np.sqrt(mass0*omega/2)-1j*pmat_eig.copy()/np.sqrt(mass0*omega*2)

# define the population on the left/right well
x_barrier = 0.37321768
P_R = np.heaviside(xgrid-x_barrier,1)
P_L = 1 - np.heaviside(xgrid-x_barrier,1)

P_R_eig = np.zeros((Neig,Neig),dtype=np.complex128)
P_L_eig = np.zeros((Neig,Neig),dtype=np.complex128)
for i in range(Neig):
    for j in range(Neig):
        P_R_eig[i,j] = np.dot(np.multiply(psi_DW[:,i].conj(),P_R),psi_DW[:,j])*dx
        P_L_eig[i,j] = np.dot(np.multiply(psi_DW[:,i].conj(),P_L),psi_DW[:,j])*dx
```

S.6.4 Dynamics: Classical and Matrix-Exponential

We propagate with thermal damping using both QuTiP and the matrix-exponential method; the latter also stores $G(t)$ and states for later quantum emulation.

Script S.6.4: Simulate the dynamics of the double-well 🔗

```python
# propagate using QuTiP
gamma1 = np.sqrt(kappa*(nth+1))
gamma2 = np.sqrt(kappa*(nth))
time_qtp = np.linspace(0,1000/pa.au2fs,20000)

# run the dynamics with different eigenstates truncation
result_qtp = {}
for N_eig_use in [20,30,40]:
    c_ops = [gamma1*Qobj(amat_eig[:N_eig_use,:N_eig_use]),
     gamma2*Qobj(adegmat_eig[:N_eig_use,:N_eig_use])]
    obs = [Qobj(P_R_eig[:N_eig_use,:N_eig_use]),
     Qobj(P_L_eig[:N_eig_use,:N_eig_use])]
    result_qtp[N_eig_use] = mesolve(Qobj(H_dw[:N_eig_use,:N_eig_use]),
                            Qobj(rho0[:N_eig_use,:N_eig_use]),
                            time_qtp, c_ops, obs,
                            options={"progress_bar": "text"}).expect

# propagation using matrix exponential propagation
N_eig_use=30
c_ops = [gamma1*amat_eig[:N_eig_use,:N_eig_use],
    gamma2*adegmat_eig[:N_eig_use,:N_eig_use]]
observable = P_R_eig[:N_eig_use,:N_eig_use]

time_short = np.linspace(0,1000/pa.au2fs,30) #compare to QuTiP time scale
result_s = propagate_matrix_exp(H_dw[:N_eig_use,:N_eig_use],
    rho0[:N_eig_use,:N_eig_use],
                        time_short, c_ops, observable, Is_show_step=True)

time_long = np.linspace(0,20000/pa.au2fs,60) #long time propagation
result_dw_l = propagate_matrix_exp(H_dw[:N_eig_use,:N_eig_use],
    rho0[:N_eig_use,:N_eig_use],
                        time_long, c_ops, observable,
                        Is_store_state = True, Is_show_step=True, Is_Gt=True)
```

S.6.5 Same Workflow with QFlux Abstractions

Script S.6.5: Simulating double-well dynamics with QFlux

```python
# ==================classical simulation===========================
# propagate using QuTiP
gamma1 = np.sqrt(kappa*(nth+1))
gamma2 = np.sqrt(kappa*(nth))

time_qtp = np.linspace(0,1000/pa.au2fs,20000)

# Double_Well with different eigenstates truncation
dw_eig = {}
result_qtp = {}
for N_eig_use in [20,30,40]:
    c_ops = [gamma1*amat_eig[:N_eig_use,:N_eig_use],
     gamma2*adegmat_eig[:N_eig_use,:N_eig_use]]
    dw_eig[N_eig_use] = DynamicsOS(Nsys = N_eig_use, Hsys =
     H_dw[:N_eig_use,:N_eig_use], \
                                    rho0 = rho0[:N_eig_use,:N_eig_use], c_ops = c_ops)

    obs = [P_R_eig[:N_eig_use,:N_eig_use], P_L_eig[:N_eig_use,:N_eig_use]]
    result_qtp[N_eig_use] = dw_eig[N_eig_use].propagate_qt(time_qtp, obs, \
                                    options={"progress_bar": "text"})

# propagate using matrix exponential propagation
N_eig_use=30
c_ops = [gamma1*amat_eig[:N_eig_use,:N_eig_use],
    gamma2*adegmat_eig[:N_eig_use,:N_eig_use]]
observable = P_R_eig[:N_eig_use,:N_eig_use]

time_short = np.linspace(0,1000/pa.au2fs,30) #compare to QuTiP time scale
result_s = dw_eig[N_eig_use].propagate_matrix_exp(time_short, observable,
    Is_show_step=True)

time_long = np.linspace(0,20000/pa.au2fs,60) #long time propagation
result_dw_l = dw_eig[N_eig_use].propagate_matrix_exp(time_long, observable, \
                        Is_store_state = True, Is_show_step=True, Is_Gt=True)
```

S.6.6   Quantum Emulation Using Stored Propagators

We expand stored propagators to a qubit-compatible dimension and run shot-based simulations.

Script S.6.6: Quantum simulation of double-well with QFlux 🔗 🐍

```python
from qflux.open_systems.quantum_simulation import expand

# ===============Quantum Simulation ======================================
dim_dw = 32

# initial state of the double-well in the dilated space
ini_occu = np.zeros(dim_dw,dtype=np.complex128)
ini_occu[5] = 1.0
rho0 = np.outer(ini_occu,ini_occu.conj())

# hamiltonian
Hsys = H_dw[:dim_dw,:dim_dw]

# collapse operator and observable
c_ops = [gamma1*amat_eig[:dim_dw,:dim_dw], gamma2*adegmat_eig[:dim_dw,:dim_dw]]
observable = P_R_eig[:dim_dw,:dim_dw]

# extract the propagator from result of classical simulation,
# and expand to match the dimension of qubit space
# For saving calculation, only choose some time points
ilarge = 5
nsteps = int(len(time_long)/ilarge)
time_qdw = np.zeros(nsteps)
Gprop_dw = []

for i0 in range(nsteps):
    i = i0*ilarge
    org_dim = result_dw_l.density_matrix[i].shape[0]
    Gprop_dw.append(expand(result_dw_l.Gprop[i],org_dim,dim_dw))

    time_qdw[i0] = time_long[i]

# double well instance
dw_quantum = QubitDynamicsOS(rep='Kraus', Nsys=dim_dw, Hsys=Hsys, rho0=rho0, c_ops
    = c_ops)
dw_quantum.set_observable(observable)
```

```
# running the quantum simulation
P_dw_qc = dw_quantum.qc_simulation_kraus(time_qdw, shots=2000,  Gprop = Gprop_dw,
    tolk = 1E-2, tolo = 5E-3)
```

S.6.7 Propagator Expansion and Kraus Reconstruction

For completeness, the helper below expands a smaller superoperator into a larger block-embedded one. We then convert the expanded $G(t)$ into Kraus operators using the method of Section S.1.

Script S.6.7: The double-well propagator 🔗 🐍

```python
def expand(Gmat_org,Norg,Nexpand):
    Gnew = np.zeros((Nexpand**2,Nexpand**2),dtype=np.complex128)
    for i in range(Norg):
        for j in range(Norg):
            for k in range(Norg):
                for l in range(Norg):
                    Gnew[i*Nexpand+j,k*Nexpand+l] = Gmat_org[i*Norg+j,k*Norg+l]
    return Gnew

dim_dw = 32
Nqb_dw = int(np.log2(dim_dw))

# extract the propagator from result of classical simulation
Gprop_dw = []
for i in range(len(result_dw_l.Gprop)):
    org_dim = result_dw_l.density_matrix[i].shape[0]
    Gprop_dw.append(expand(result_dw_l.Gprop[i],org_dim,dim_dw))
```

Next, we apply the technique from Section S.1 to convert the propagator into the Kraus operator representation. After running the code in Script S.6.8, we obtain the Kraus operators $M_i(t)$ that describe the evolution of the system from time 0 to time t.

Script S.6.8: Obtaining Kraus operators from the propagator 🔗 🐍

```python
# For saving calculation, only choose some time points
ilarge = 5
nsteps = int(len(Gprop_dw)/ilarge)

Kraus_all = {}
for i0 in range(nsteps):
    i = i0*ilarge
    print('istep: ',i0)

    # get the kraus operators from the propagator
    Kraus_all[i0] = gen_Kraus_list(Gprop_dw[i],dim_dw,tol=1E-2)
```

S.6.8 Initial State, Observable, and Pauli Decomposition

We prepare the dilated initial state and decompose the observable into Pauli strings for estimator-based expectation evaluation.

Script S.6.9: Initial state and observable 🔗 🐍

```python
from qflux.open_systems.trans_basis import ham_to_pauli
from qiskit.quantum_info import SparsePauliOp
import numpy as np

# initial state of the double-well in the dilated space
ini_occu = np.zeros(dim_dw,dtype=np.complex128)
ini_occu[5] = 1.0
stat0_dil = np.concatenate((ini_occu,np.zeros(dim_dw)))


# decompose the dilated space observable into summation of tensor product of pauli
    matrices
Obs_mat = np.zeros((2*dim_dw,2*dim_dw),dtype=np.complex128)
Obs_mat[:dim_dw,:dim_dw] = P_R_eig[:dim_dw,:dim_dw]
Obs_paulis_dic = ham_to_pauli(Obs_mat, Nqb_dw+1, tol=5E-3)

# Prepare the qiskit observable from the pauli strings of observable matrix
data = []
coef = []
```

```
    for key in Obs_paulis_dic:
        data.append(key)
        coef.append(Obs_paulis_dic[key])
    obs_q = SparsePauliOp(data,coef)
```

S.6.9 Quantum Simulation with Kraus-Dilated Unitaries

Finally, we loop over times, apply each (dilated) Kraus operator to the prepared state, and estimate the observable using `Estimator`. The sum over Kraus paths yields the expected population on the right well.

Script S.6.10: Quantum Simulation of Double-Well 🔗

```python
from qiskit_aer.primitives import Estimator

# Aer implementation of an Estimator
estimator = Estimator()

shots = 2000

# For saving calculation, only choose some time points
ilarge = 5
nsteps = int(len(Gprop_dw)/ilarge)

time_dw_qc = np.zeros((nsteps),dtype=np.float64)
P_dw_qc = np.zeros((nsteps),dtype=np.float64)

for i0 in range(nsteps):

    i = i0*ilarge

    time_dw_qc[i0] = time_long[i]
    matKraus_list = Kraus_all[i0]
    print('istep: ', i0, 'Length: ', len(matKraus_list))

    for ikraus in range(len(matKraus_list)):

        # Create the quantum circuit
        qr = QuantumRegister(Nqb_dw+1)
```

```
cr = ClassicalRegister(Nqb_dw+1)
qc = QuantumCircuit(qr, cr)

# Initialize the quantum circuit with the initial state
qc.initialize(stat0_dil, qr)

# Create a custom unitary operator with the dilated Kraus propagator
UM = dilate(matKraus_list[ikraus],Isscale=False)
UM_op = Operator(UM)

# Apply the unitary operator to the quantum circuit's qubits
qc.unitary(UM_op, qr)

result = estimator.run(qc, obs_q, shots = shots).result()
P_dw_qc[i0] += result.values[0]
```